Numerical Modeling of Reinforced Concrete Moderate Aspect-Ratio Walls

By

Abraham Bahre

Masters project Submitted as partial fulfillment of the requirements for the degree of Master of Science in Civil Engineering

Academic Advisor

Dr. Serhan Guner

Department of Civil Engineering

University of Toledo

December 2017

ABSTRACT

Reinforced concrete moderate aspect-ratio walls are commonly used in high-rise buildings. Past studies have shown that such walls are expected to yield in flexural first, however, nonlinear shear interaction significantly reduces the strength, stiffness, and ductility of the wall. In this project, a numerical modeling of moderate aspect-ratio reinforced concrete walls that compare global nonlinear flexural and shear responses, and horizontal displacement at the top of the wall was carried out in OpenSees and VecTor5. A total of ten RC wall experimental tests were done in the past where from three different research programs are selected to model in this project which are divided into two parts. Part I of this project describes the analytical modeling of the RC walls under monotonic loading and the verification of this numerical modeling is completed based on a comparison of load versus deflection curve with experimental responses. Part II of this project describes the numerical modeling under constant axial load and reverse cyclic loading condition and effect of shear on moderate aspect-ratio RC walls and flexural capacity was achieved. In the nonlinear analysis of this project, a two-dimensional Multiple-Vertical-Line-Element-Model (MVLEM) formulation implemented in OpenSees platform was used. And also smeared, rotating crack approach based on the Modified Compression Field Theory (MCFT) and the Disturbed Stress Field Model (DSFM) formulation implemented on VecTor5 was used.

Table of Contents

Introduction

1.1 General

Reinforced concrete structural walls are one of the most commonly employed lateral-load resisting systems for mid- and high-rise buildings (e.g., core wall system or wall-frame dual systems). They are relatively stiff and strong; thus, their use results in relatively less floor area of the building being reserved for lateral-load resisting structural elements. Additionally, they are easily incorporated into the architectural layout of mid and high-rise buildings by placing them in the interior of the buildings around elevators. A typical concrete high-rise building has core shear walls located near the center of the building plan and has perimeter columns to support the flat plate floor slabs.

Architectural advantages of concrete shear wall buildings over concrete frame buildings are.

(I) the absence of large moment-resisting frames on the outside of the building means that larger windows can be provided around the entire exterior of shear wall buildings,

(II) (II) The construction of concrete shear wall buildings is also known to be very competitive because simpler formwork and less congested reinforcement lead to lower labor costs and generally faster construction.

Reinforced concrete walls are designed to carry flexural, shear and axial loads. And their behavior generally classified according to their aspect-ratio, defined as the ratio of the wall height to wall length (h_w / l_w)or shear-span to depth ratio (M /Vl_w). If walls have an aspect-ratio (AR), that is small (less than 1.5), they are typically referred to as squat. If walls have an AR that is large (greater than 2), they are typically referred to as slender (Birely 2012). If walls have an AR between approximately 1.5 and 2.5 they typically referred as moderate aspect-ratio wall **(**Orakcal and Wallace 2006).

Squat walls typically carry relatively higher shear stress demands and exhibit shear-dominated response. Shear-dominated response would include shear deformation accounting for a significant portion of the total deformation, development of diagonal cracks through the web and boundary regions of the wall, development of diagonal or horizontal zones of concrete crushing within the web that may extend into the boundary regions of the wall, and possibly not achieving the nominal flexural strength of the wall. Squat walls typically exhibit lower ductility capacity.

Slender walls typically carry relatively lower shear stress demands and exhibit flexure-dominated response. Flexure-dominated response would include flexural deformation accounting for a relatively large portion of the total deformation, development of horizontal flexural cracks in the boundary regions of the wall, development of diagonal shear cracks within the web of the wall, loss of lateral load carrying capacity due to compressive failure of a boundary region (crushing of core concrete and buckling of longitudinal steel) or due to fracture of longitudinal steel (Birely 2012).

Moderate-aspect-ratio walls- that is, walls with aspect-ratios between approximately 1.5 and 2.5 although flexural yielding is expected, nonlinear shear behavior may be significant, potentially leading to lower strength, stiffness, and ductility (Massone et al. 2004), and larger concrete compressive strains at the wall edge (Orakcal and Wallace, 2004). Experimental results have shown that flexural and shear yielding occur near-simultaneously even when the wall nominal shear strength is as much as twice the shear developed at flexural yielding, suggesting that there is an interaction between nonlinear flexural and shear modes of behavior, commonly referred to as shear-flexure interaction (SFI) (Massone and Wallace 2004).

Flexure, shear, and axial demands are used to design the geometry of the wall as well as the layout of longitudinal reinforcing steel, horizontal and commentary (ACI 318 2014), referred to as the ACI Code. In the US, shear demand on the wall typically determines the gross area of the wall, as the ACI Code requires that the shear strength reinforcing steel, and transverse, confining steel placed in the boundary regions of the wall. In the US, walls design is typically one in accordance with the American Concrete Institute building code requirements for structural concrete of a wall not exceed $8\sqrt{f'_c}\,A_{CV}$, where f'_c is the concrete compressive strength in psi and Acv is the area, in square inches, of the wall that is expected to carry shear. Horizontal reinforcement is designed (bar size and spacing) based on the shear demand. Longitudinal reinforced is designed (bar size and spacing) based on the flexural and axial load demands. Often longitudinal reinforcement is concentrated at the ends of a planar wall (corners of a c-shaped wall), with the ACI code minimum longitudinal reinforcement distributed within the interior, or web, of the wall; this reinforcement layout is more efficient for planar walls. Finally, for walls in regions of high seismicity, transverse reinforcement is designed to confine concrete and delay buckling of longitudinal steel at the ends of a planar wall (regions expected to experience high compressive strain demands for non-planar walls). To reduce the likelihood of walls exhibiting less ductile, shear-dominated failure;

significantly lower resistance factors are defined for shear strength than for flexural strength. Additional ACI Code requirements address minimum longitudinal and horizontal reinforcement ratios as well as specifications for detailing of confined boundary regions, with the intent of ensuring that walls exhibit acceptable performance under service-level loads and in the event of design-level earthquake loading (Birely 2012).

1.2 Objective

The behavior of shear walls is primarily affected by a combination of flexural, shear and axial deformations. Medium- to high-rise wall are mostly controlled by flexural deformations, while low-rise walls are controlled mainly by the shear deformations. In the past decades, experimental tests on RC shear walls showed that their nonlinear response may vary according to several factors. Some of these factors are:

1- The wall dimensions and its aspect-ratio.
2- The axial load level applied to the wall (axial-flexure interaction).
3- Reinforcement percentage and the bond between the reinforcement and concrete.
4- The wall flexure capacity relative to the wall shear capacity.
5- Rigidity of wall foundation.
6- The effect of the structural elements connected to the wall (e.g. coupling beams, moment resisting frame, etc.).

Thus, modeling of RC shear walls should consider, especially for the shear-flexure interaction to simulate the wall behavior efficiently. The analytical model should be able to capture the monotonic capacity of the wall, as well as its behavior under reversed cyclic loading. In the past decades, various modeling approaches that have been used by researchers in the modeling of RC shear walls to capture and observe nonlinear flexural, shear and axial behavior were done. Majority of the researchers used approaches based on the use of fiber-type models with interaction incorporated through biaxial representation of concrete behavior (e.g., MCFT (Vecchio and Collins 1986), within each macro-fiber, such as models proposed by (Massone et al. 2006, 2009), (Jiang and Kurama 2010), and (Fischinger et al. 2012). (Massone et al. 2006, 2009) provided comparisons of model predictions against experimental results for cantilever walls with the aspect-ratio (shear-span-to-depth ratio) of 3.0 (Thomsen and Wallace 1995), as well as for squat wall segments with the shear-span-to-depth ratio of 0.5 (Massone et al. 2009). (Jiang and Kurama

2010), provided comparisons between the predictions of their analytical modeling approach and experimental results for a wall specimen with aspect-ratio of 2.4 (Oesterle et al. 1979),; however, the comparisons were presented for only lateral-load-versus-top-displacement responses and for tensile strains in boundary longitudinal reinforcement, both of which are not expected to be notably sensitive to shear-flexural interaction(SFI) for a relatively moderate aspect walls (Orakcal and Wallace 2006). A methodology based on a strut-and-tie (truss) modeling approach proposed by (Panagiotou et al. 2011), has been shown to be a viable method to capture SFI; however, due to overlapping areas of vertical, horizontal, and diagonal concrete struts in the model, achieving accurate displacement responses over a broad range of response amplitudes is a challenge. In addition, strut angles are pre-defined and do not change during the analysis, which may allow for reasonably comparisons with tests on isolated cantilever walls, but does not address variation in strut angles due to changes in axial load for walls with some degree of coupling (Kolozvari et al. 2015).

In general modeling of RC shear wall available have the following shortcoming

1. Modeling has empirical or semi-empirical formulations
2. Most of the modeling have capable of simulation monotonic response only
3. Models have not been implemented in computational platforms like OpenSees
4. Models have not been expressively validated against global and local response

According to **ACI _445B_SHEAR WALL DATA BASE** file, a total of 508 different aspect-ratio shear walls were tested by different researchers. 185 (36%) of the total were done for Squat walls that has aspect-ratio AR less than 1.5, 75 (14.7%) were slender walls with AR greater than 2.5 and 65 (12.7%) were done for moderate aspect-ratio with AR 1.5-2.5. And in this file 192 (37.7 %) walls were reported in the Chinese language.

Given the above shortcoming, and due to few test done on moderate aspect-ratio, in this paper a project of total 10 moderate-aspect-ratio reinforced structural wall specimens from three experimental research programs will be modeled using MVLEM approaches to study the cyclic Shear-Flexural Interaction in OpenSees (Mckenna et al. 2000), and VecTor5 (Guner 2008).

The specimens were selected based on the following criteria

1. Planar (rectangular) wall specimen subjected to in-plane flexure, shear, and axial loading,

2. Data required to define a numerical model were provided. Required data included concrete compressive strength, reinforcing steel stress-strain response, specimen geometry, reinforcement layout, and test specimen boundary conditions in the laboratory.

1.3 Analytical Model

1.3.1 OpenSees: Multiple-Vertical-Line-Element Model (MVLEM)

This model was first introduced by (Vulcano et al. 1988). In this model as shown in As shown in Figure 1.1(a)), the wall element was represented by a number of uniaxial elements connected in parallel using infinitely rigid bars located at the top and bottom wall ends; two external elements simulate the wall boundary elements, while the other elements simulate the combined axial-flexure behavior of the central panel. A horizontal spring was used to represent the inelastic shear behavior of the wall. The authors modified the axial-element-in-series model (AESM) by having a two-component model for element 1, representing the cracked concrete and steel reinforcement behavior, instead of the one-component element in the original model as shown in Figure 1.1 (b). The constitutive laws for concrete (cracked and uncracked) and steel elements were defined to describe the hysteretic response of the materials. It was concluded that the model predicted the flexural behavior of the wall efficiently even when relatively few uniaxial elements were used (4 elements). It is worth noting that, although the proposed model considered both flexural and shear behavior, their responses were not coupled. (Colotti 1993), modified the MVLE model to include the interaction between axial and shear responses, which led to a more accurate simulation. Simpler constitutive laws and some modifications to the MVLE were introduced by (Fischinger et al 1990), and by (Orakcal and Wallace 2004), to improve the efficiency of the model in predicting the response of RC shear walls without sacrificing the accuracy.

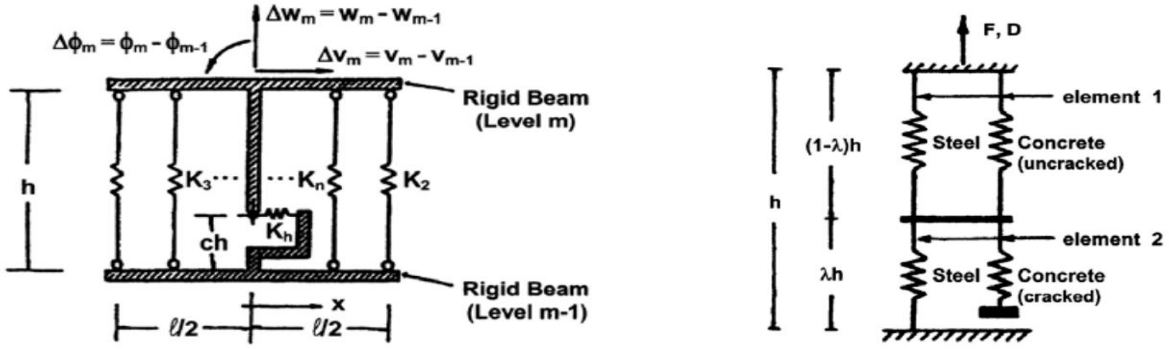

Figure 1.1. (a) MVLEM (Vulcano et al. 1988); (b) Modified axial-element-in-series model.

(Orakcal and Wallace 2006), employ standard one-dimensional cyclic constitutive models to define the response of concrete and steel fibers and an elastic shear response model. They show that the MVLEM can provide an accurate simulation of wall response for walls for which the assumptions of plane sections remain plane, elastic shear response, and decoupling of flexure and shear response are valid (Pugh et al 2015).

1.3.1.1 Formulation for MVLEM

According to (Orakcal and Wallace 2004), a structural wall is modeled as a stack of ***n*** MVLEM elements, which are placed on one another. The flexural response is simulated by a series of uniaxial elements (or microfibers) connected to rigid beams at the top and bottom (for example, floor) levels. The stiffness properties and force-displacement relationships of the uniaxial elements are defined according to state-of-the-art, uniaxial, cyclic constitutive models for concrete and steel and the tributary area assigned to each uniaxial element. The number of the uniaxial elements ***n*** can be increased to obtain a more refined description of the wall cross-section.

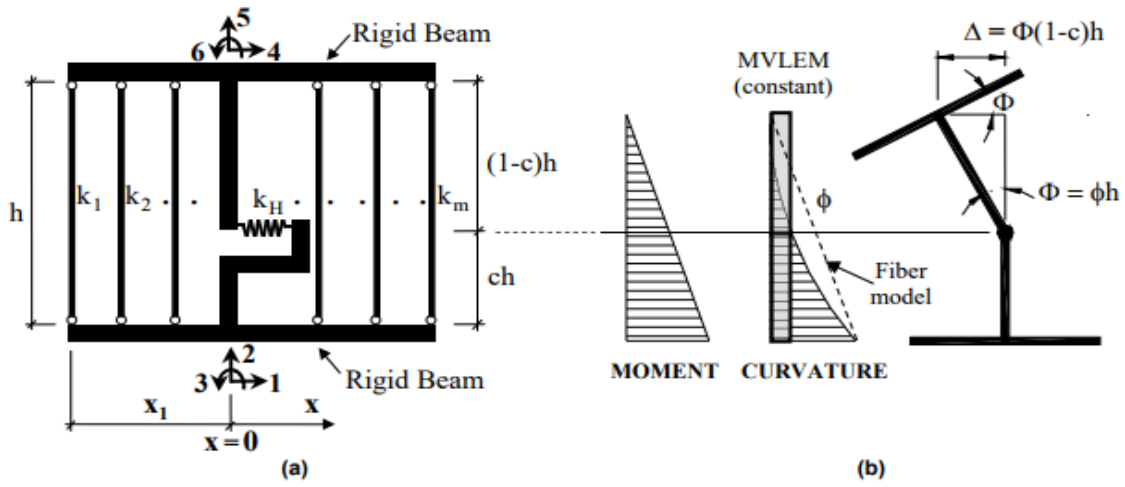

Figure 1.2 (a) MVLEM element Model element formulation and; (b) Rotations and displacements.

The relative rotation between the top and bottom faces of the wall element occurs around the point placed on the central axis of the element at height ch as shown in (Figure 1.2). Rotations and resulting transverse displacements are calculated based on the wall curvature, derived from the section and material properties, corresponding to the bending moment at that specific point of each element. A suitable value of the parameter ***c*** is based on the expected curvature distribution along the element height ***h***. A value of ***c*** = 0.4 was recommended by (Vulcano, Bertero, and Colotti

1988), based on a comparison of the model response with experimental results. Selection of **c** becomes important in the inelastic range, where small changes in the moment can yield highly nonlinear distributions of curvature. Stacking more elements along the wall height, especially in the regions where inelastic deformations are expected, will result in smaller variations in the moment and curvature along the height of each element, thus improving analytical accuracy.

A horizontal spring placed at the height ***ch***, with a nonlinear hysteretic force-deformation behavior following an origin-oriented hysteresis model (OOHM)deformation rule was originally suggested by (Vulcano, Bertero, and Colotti1983 to simulate the shear response of the wall element. The OOHM was proven to be unsuitable by (Vulcano and Bertero 1987), for an accurate idealization of the shear hysteretic behavior especially when high shear stresses are expected, however, focuses on modeling and simulation of the flexural response, thus a linear elastic force-deformation behavior was adopted for the horizontal "shear" spring. Flexural and shear modes of deformation of the wall member are uncoupled (that is, inelastic flexural deformations do not affect shear strength and inelastic shear deformation), and the horizontal shear displacement at the top of the element does not depend on ***c.***

1.3.1.2 Material Constitutive Models

The stiffness and force-deformation properties of the uniaxial elements are derived from uniaxial stress-strain material behavior; therefore, various state-of-the-art uniaxial material constitutive models can be implemented. Axial models for reinforcing bar buckling and bond slip can also be incorporated into the wall model because the stiffness properties of the wall model are based on axial force-deformation relationships. Responses obtained using the present wall model were found to be sensitive to the material constitutive models used; therefore, details of the constitutive laws used in this study for steel and concrete are described in the following sections.

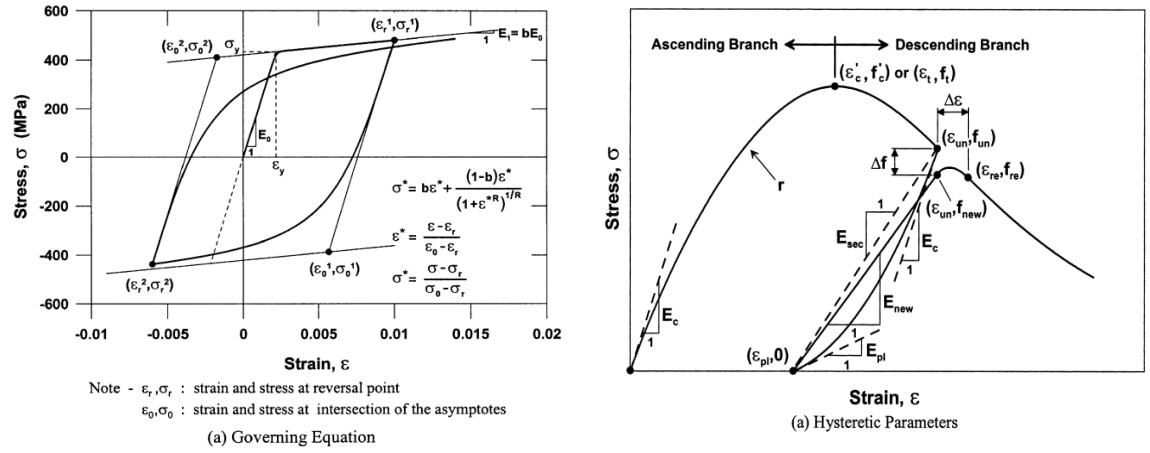

Figure 1.3 (a) Steel Constitutive model; (b) Concrete constitutive model; (Chang and Mander 1994).

1.3.2 VecTor5: Modified Compression Field Theory (MCFT) and Disturbed Stress Field Model (DSFM)

VecTor5 is a nonlinear sectional analysis program for two-dimensional frame-related structures consisting of beams, columns and shear walls, subjected to temperature, static and dynamic loading conditions. Temperature loads include nonlinear thermal gradients; static loads include monotonic, cyclic and reversed-cyclic load cases; dynamic loads include base accelerations (time-history analysis under an input accelerogram), impulse, impact and blast loads, initial velocity and constant acceleration load cases. Based on the Modified Compression Field Theory (Vecchio and Collins, 1986), and the (Vecchio, 2000), VecTor5 uses a smeared, rotating crack approach for reinforced concrete based on a total load, secant stiffness formulation (user's manual od VeTor5 by Guner 2008).

In this study a layered section approach is used to determine the response of each reinforced or prestressed concrete section to thermal and mechanical loads by dividing the cross section into a number of concrete layers, longitudinal reinforcing bar layers and longitudinal restressing steel layers as shown in (Figure 1.4).

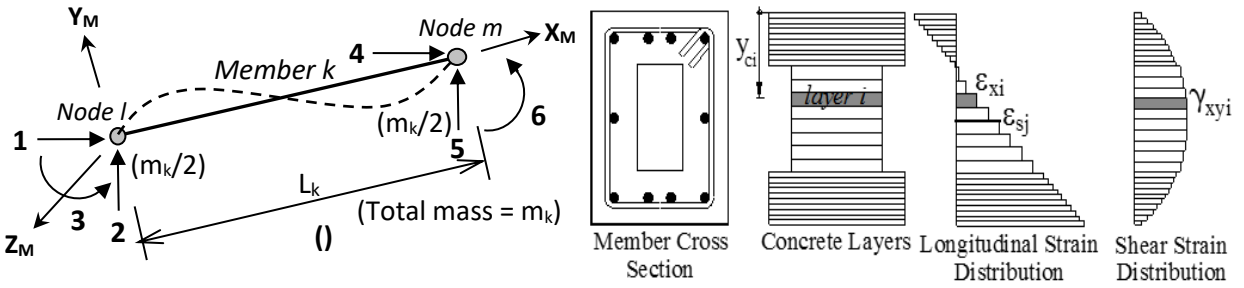

Figure 1.4 Input parameters for sectional analysis of VecTor5 (Guner 2008).

f'_c is the concrete compressive strength,

ρ_{ti} and ρ_{zi} are the transverse and out-of-plane reinforcement ratios respectively,

S_{ti} is the spacing of the transverse reinforcement in the longitudinal direction,

f_{yi} and f_{ui} are the yield and ultimate stresses of the transverse reinforcement respectively,

E_{sti} and E_{shti} are the Young's and the strain hardening moduli of the transverse reinforcement,

ε_{shti} is the strain at the onset of strain hardening,

A_{sj} is the total cross-sectional area of the longitudinal reinforcement, and

$\Delta_{\varepsilon pj}$ is the locked-in strain for a prestressing steel layer.

Then each concrete and steel layers are analyzed individually based on the MCFT or the DSFM, (Vecchio 2000), although sectional compatibility and sectional equilibrium conditions are satisfied as a whole. The main sectional compatibility requirement enforced is that "plane sections remain plane," which permits the calculation of the longitudinal strain in each layer of concrete, reinforcing, and prestressing steel layer as a function of the top and bottom fiber strains, as shown in Figure 1.4. (Guner 2010).

At the end of the analysis, the procedure provides sufficient output to fully describe the behavior of the structure, including the load-deflection response, member deformations and deflections, concrete crack widths, reinforcement stresses and strains, deficient parts and members (if any), and failure mode and failure displacement of the structure. The post-peak response of the structure is also provided, through which the energy dissipation and the displacement ductility can be calculated

PART I: Monotonic Loading

The main purpose of doing Part I of this project is monotonic loading analysis, which is done to capture and estimate the ultimate loading capacity of the RC walls and to do so we used Multiple-Vertical-Line-Element-Model (MVLEM) approach which is implemented in OpenSees and compare the deflection response with experimental results and numerical modeling using VecTor5.

2.1 Thien A. Tran and John W. Wallace 2015

2.1.1 Experimental Program

Three of approximately one-half-scale reinforced concrete structural wall specimens tests done were selected in this project which are subjected to combined constant axial load and reversed cyclic lateral loading, were tested as shown in (Table 1). Specimen identifiers are used for quick reference, i.e., specimen RW-A1.5-P10-S51, describes a rectangular wall with the aspect-ratio of 1.5 under design axial load P of 10%Ag f'_c, and design average shear stress of 3.8 f'_c psi (0 3. 2 f'_c MPa). The three wall specimens were 6 in. (150 mm) thick and 48 in. (1220 mm) long, with the lateral load, applied at either 72 or 96 in. (1830 and 2440 mm) above the wall-foundation interface. Dimensions and reinforcement details of all three specimens are given in Figure 2.1. It is noted that the boundary longitudinal reinforcement used for the roughly one-half scale test walls was either U.S. No. 4, 5, and 6 (approximately U.S. No. 8, 10, and 11 for the prototype walls) and that clear concrete cover over boundary transverse reinforcement for the test walls varied from 0.5 in. (12.7 mm) for No. 6 boundary longitudinal reinforcement to 0.625 in. (15.9 mm) for No. 4 boundary vertical reinforcement. Axial load levels of 0.10Ag f'_c were applied to the three walls, where f'_c was the design concrete compressive strength. The ratios of horizontal and vertical web reinforcement of each wall ρ_h and ρ_v, respectively were equal and exceeded the 0.0025 minimum required by ACI 318-11. The ratio ρ_b of the area of vertical boundary reinforcement to the boundary element area varied between 3.23% and 6.06. (Tran and Wallace 2015).

Table 2.1 Wall specimen parameters (Tran and Wallace 2015).

specimen ID	Author	h/lw	thickness(	f'c		fy		ρflex %	ρh, %	ρv, %
				Mpa	psi	Mpa	KSI			
RW-A15-P10-S51	Tran and Wallace 2015	1.5	150	48.8	7077	477	69.2	3.23	0.32	0.32
RW-A15-P10-S78	Tran and Wallace 2015	1.5	150	57.5	8340	477	69.2	6.06	0.61	0.61
RW-A2.0-P2.5-S38	Tran and Wallace 2015	2	150	57.5	8340	477	69.2	6.06	0.61	0.61

Where

ρ_{flex}: the ratio of main flexural reinforcement to the gross concrete area.

ρ_h: the ratio of horizontal reinforcement to the gross concrete area.

ρv: the ratio of vertical web reinforcement to the gross concrete area.

2.1.1.1 Material properties

Concrete clear cover over boundary longitudinal reinforcement was selected to be greater than or equal to one longitudinal boundary bar diameter (either U.S. No. 4, 5, or 6); therefore, a maximum aggregate size of 3/8 in. (9.5 mm) was specified to alleviate concerns related to concrete placement (consolidation). For each wall specimen, three concrete cylinders were tested to obtain stress-versus-strain relations and average compressive strength (Table 2.2).

Table 2.2 Yield and ultimate strengths of reinforcement (Tran and Wallace 2015).

Bar	No. 2	No. 3	No. 4	No. 5	No. 6	D6a	D6b
Diameter, mm (in.)	6.4 (0.25)	9.5 (0.375)	12.7 (0.5)	15.9 (0.625)	19.1 (0.75)	6.0 (0.236)	6.0 (0.236)
Cross-sectional area, mm² (in.²)	31.7 (0.049)	71.3 (0.11)	126.7 (0.20)	197.9 (0.31)	285.0 (0.44)	28.3 (0.044)	28.3 (0.044)
Yield strength, MPa (ksi)	423 (61.4)	443 (64.2)	472 (68.4)	474 (68.7)	477 (69.2)	450 (65.3)	516 (74.9)
Ultimate strength, MPa (ksi)	492 (71.3)	707 (102.6)	613 (88.9)	620 (89.9)	637 (92.4)	661 (95.9)	580 (84.2)

Deformed reinforcement consisted of eight boundary longitudinal headed bars (either No. 4, 5, or 6), whereas web reinforcement consisted of two curtains of either D6 (6 mm diameter), No. 2, or No. 3 bars. Yield and ultimate strengths of reinforcement are given in Table 2.2.

2.1.1.2 Test Procedure

The cantilever wall specimens were tested in an upright position with a quasi-static lateral load applied at a height of 8 ft. (2440 mm) above the wall-foundation interface for the aspect-ratio 2.0 specimens, and at a height of 6 ft. (1830 mm) for the aspect-ratio 1.5 specimens. Axial load was applied using two hollow-core cylinders connected to post-tensioning bars, one on each side of the wall as shown in (Figure 2.2 (a)). The lateral load was applied through a friction mechanism using two plates, one on either wall face along with through-wall post-tensioning bars, to distribute the lateral load uniformly across the top of the wall. The reversed cyclic lateral load was transmitted to the wall at a very slow rate. An out-of-plane support frame, consisting of a horizontal, planar truss and two vertical frames, was used to prevent wall twisting during testing, but allow wall lateral and vertical displacement at the top of the wall (Tran and Wallace 2012).

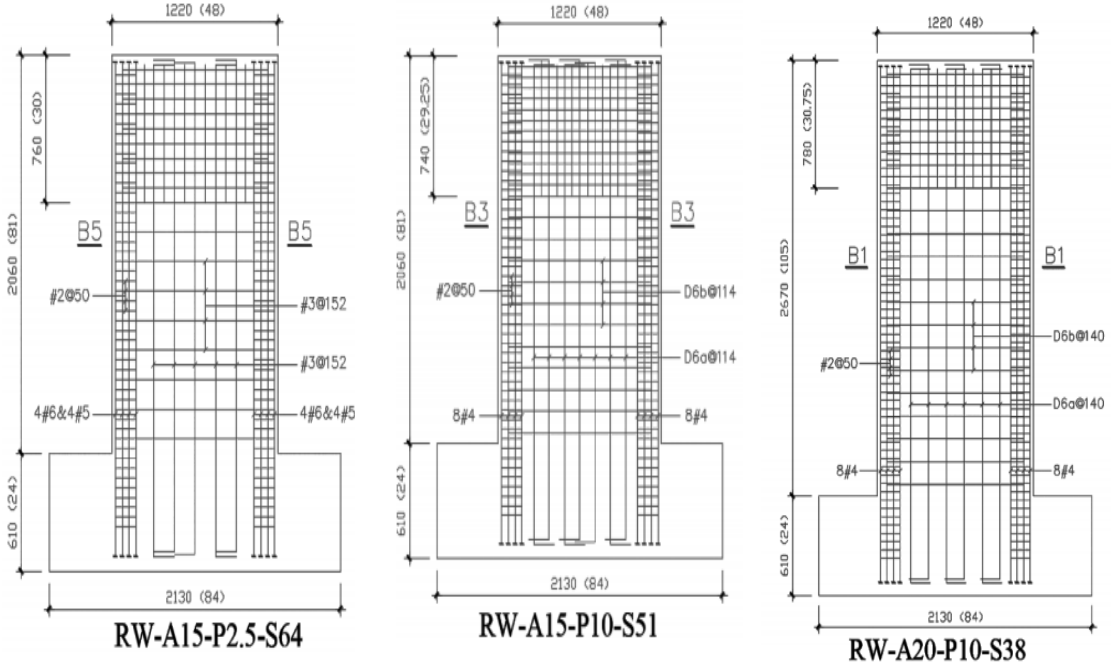

Figure 2.1 Dimensions and reinforcement details of wall specimens. (Units in mm; 1 in=25.4 mm.).

The testing protocol consisted of load-controlled cycles, generally three cycles at one-fourth, one-half, and three-fourths of the expected yield force, followed by displacement controlled cycles, typically three cycles at top drift ratios of 0.375%, 0.5%, 0.75%, 1.0%, 1.5%, 2.0%, and two cycles at top drift ratios of 3.0% and 4.0%.

2.1.2 Modeling using OpenSees

To predict the maximum load capacity of moderate aspect RC walls, three RC wall specimen (Tran and Wallace 2015) tested under constant axial load and cyclic lateral displacement history applied at the top of the wall was predicted using the MVLEM model. Two specimens were 6 in. thick, 48 in. long, and 72 in. high, which corresponds to an aspect (or shear-span-to-depth) ratio of 1.5 (moderate-aspect-ratio wall) and the third wall was 48 in thick and 96 in high which results to 2.0 shear span to depth ration.

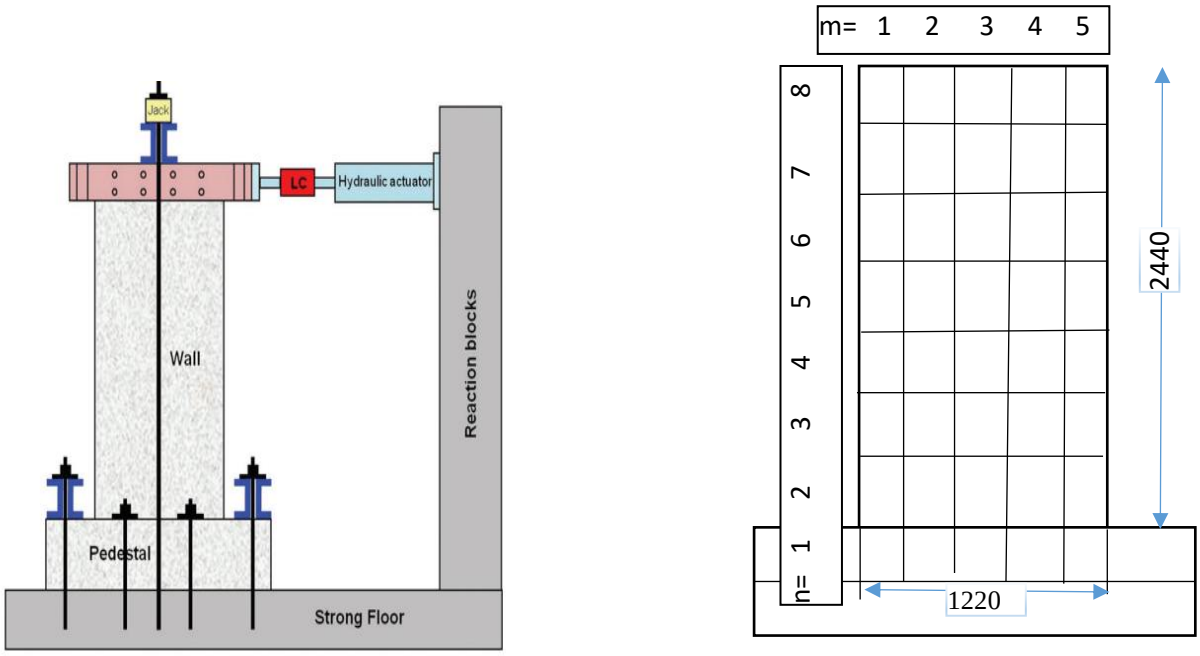

Figure 2.2 (a) Experimental test set up; (b) Model discretization in OpenSee.

The specimen was subjected to a constant axial load of approximately 10% of wall axial capacity. The nonlinear material response was defined using typical uniaxial concrete and steel response models as shown in Figure 1.3 (a) and (b) respectively. The Steel02 material model used to simulate the response of reinforcing uniaxial steel material. This model employs a bilinear envelope with unload-reload paths defined using (Menegotto and Pinto 1973), steel material object with isotropic strain hardening. Input Parameters defined in Figure 2.3 were taken directly from the experimental test reported material properties for each specimen in the database as shown in Table2.1.

uniaxialMaterial Steel02 $matTag $Fy $E $b $R0 $cR1 $cR2 <$a1 $a2 $a3 $a4 $sigInit>

$matTag	integer tag identifying material
$Fy	yield strength
$E0	initial elastic tangent
$b	strain-hardening ratio (ratio between post-yield tangent and initial elastic tangent)
$R0 $CR1 $CR2	parameters to control the transition from elastic to plastic branches. Recommended values: **$R0**=between 10 and 20, **$cR1**=0.925, **$cR2**=0.15
$a1	isotropic hardening parameter, increase of compression yield envelope as proportion of yield strength after a plastic strain of $a2*($Fy/E0). (optional)
$a2	isotropic hardening parameter (see explanation under $a1). (optional default = 1.0).
$a3	isotropic hardening parameter, increase of tension yield envelope as proportion of yield strength after a plastic strain of $a4*($Fy/E0). (optional default = 0.0)
$a4	isotropic hardening parameter (see explanation under $a3). (optional default = 1.0)
$sigInit	Initial Stress Value (optional, default: 0.0) the strain is calculated from epsP=$sigInit/$E if (sigInit!= 0.0) { double epsInit = sigInit/E; eps = trialStrain+epsInit; } else eps = trialStrain;

Figure 2.3 Steel02 uniaxial material input parameters in OpenSees.

The Concrete response was defined using uniaxial material ConcreteCM (Kolozvari et al., 2015), which is a uniaxial hysteretic constitutive model for concrete developed by (Chang and Mander 1994). This model is a refined, rule-based, generalized, and non-dimensional constitutive model that allows calibration of the monotonic and hysteretic material modeling parameters, and can simulate the hysteretic behavior of confined and unconfined, ordinary and high-strength concrete, in both cyclic compression and tension as shown in (Figure 2.4). The model addresses important behavioral features, such as continuous hysteretic behavior under cyclic compression and tension, progressive stiffness degradation associated with smooth unloading and reloading curves at increasing strain values, and gradual crack closure effects. Details of the model are available in the report by (Chang and Mander 1994).

Input Format:

uniaxialMaterial ConcreteCM $mattag $fpcc $epcc $Ec $rc $xcrn $ft $et $rt $xcrp <-GapClose $gap>

$mattag	Unique *uniaxialMaterial* tag
$fpcc	Compressive strength (f'_c)
$epcc	Strain at compressive strength (ε'_c)
$Ec	Initial tangent modulus (E_c)
$rc	Shape parameter in Tsai's equation defined for compression (r_c)
$xcrn	Non-dimensional critical strain on compression envelope (ε^-_{cr}, where the envelope curve starts following a straight line)
$ft	Tensile strength (f_t)
$et	Strain at tensile strength (ε_t)
$rt	Shape parameter in Tsai's equation defined for tension (r_t)
$xcrp	Non-dimensional critical strain on tension envelope (ε^+_{cr}, where the envelope curve starts following a straight line – large value [e.g., 10000] recommended when tension stiffening is considered)
<-GapClose $gap>	**gap** = 0, less gradual gap closure (default); **gap** = 1, more gradual gap closure

Figure 2.4 ConcreteCM uniaxial material input parameters in OpenSees.

Specimen geometry along the height was discretized using eight MVLEM elements as shown in Figure 2.2 (b). Discretization of the model cross section was performed using five RC panel elements, where the outer two fibers represented confined wall boundaries and the three inner fibers represented the unconfined web of the wall.

2.1.3 Modeling using VecTor5

For comparing the horizontal load versus displacement response, the RC walls also modeled in VecTor5. Using Formworks Plus, graphical interface, that prepares the text files required for a VecTor5 program the material properties are defined using experimental data. The concrete compressive strength, tensile strength, and other values can be input as shown in Figure 2.5 and the transverse and longitudinal reinforcement can also be defined as shown in Figure 2.6 along with cross-sections for the members that will be meshed throughout the structure.

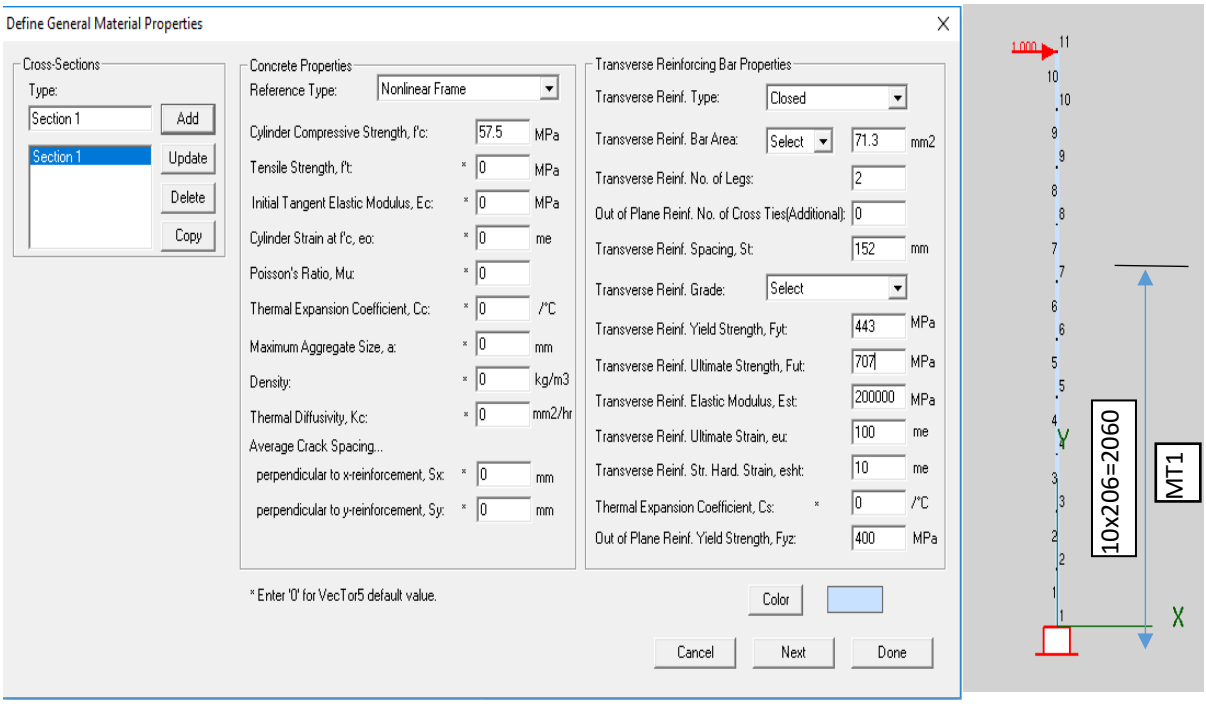

Figure 2.5 Concrete input parameters taken from Janus for (Tran and Wallace 2015).

The RC walls were subjected to a horizontal lateral load at the top of the wall with the displacement controlled mode to create the monotonic load conditions with 1 mm impressing displacement amplitude. Input parameters were taking from the experimental test data as shown in Figure 2.5. The walls were created with members that have the same length 10% of the length of the wall. For example, for wall R1.5_64 a length of 206 mm was used as shown in Figure 1.8. For shear wall

structures, (Guner 2008), recommended that member lengths in the range of 10% of the cross-section height be used. (This recommendation is based on a limited parametric study including only flexure-critical shear walls; shear-critical shear walls should also be investigated to reach a more general recommendation.). The base blocks of the walls were not considered, rather they were modeled as a fixed supporter of the wall and no rigid zone used on all analysis using VecTor5. One member material (MT1) was used with 32 concrete layers for section models as shown in Figure 2.6 (b).

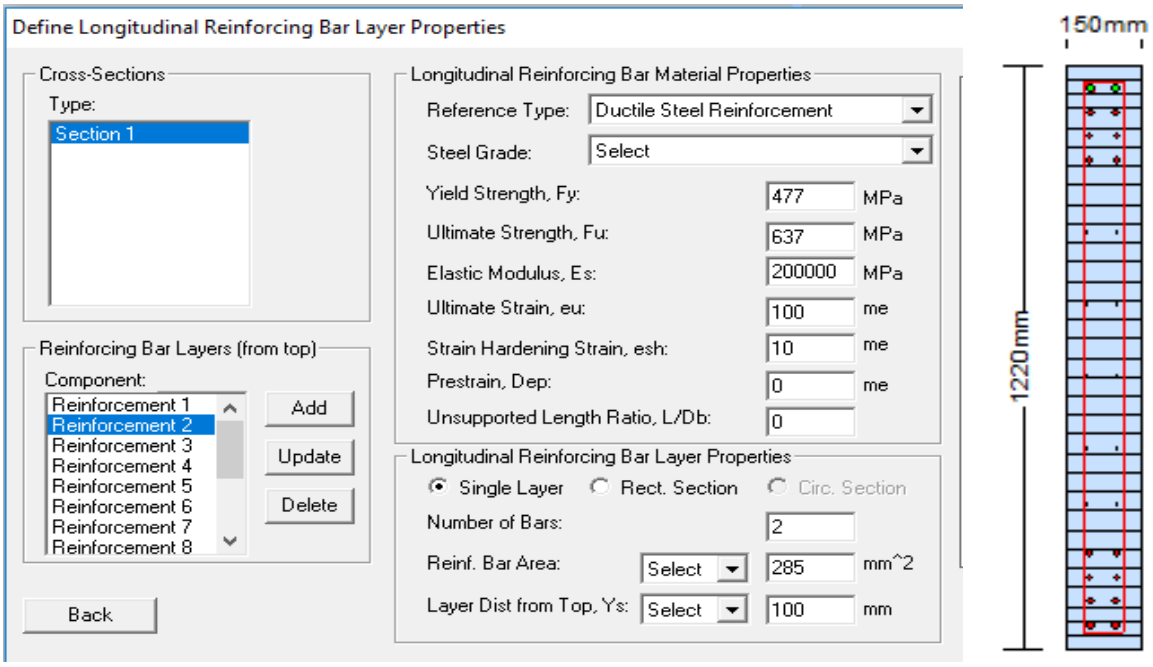

Figure 2.6 (a) Steel input parameters; (b) Concrete layers.

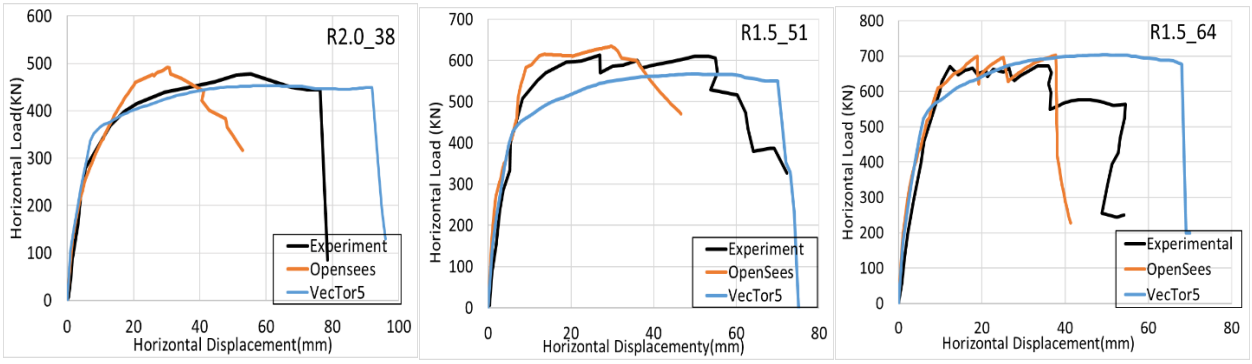

Figure 2.7 Comparison horizontal displacement (mm) vs horizontal load (KN).

As shown in Figure 2.7 the numerical modeling using OpenSees and VecTor5 captured reasonably well over all load-deformation response comparing to the experimental test done. For example,

specimen R1.5_64 a horizontal sliding along the crushed concrete zone approximately one to two wall thicknesses above the wall-foundation interface was observed during the loading, causing a substantial reduction of the wall lateral strength as shown in Figure 2.8 (a), correspondingly a horizontal shear failure was observed from VecTor5 analysis at member one which is within 206 mm as shown in Figure 2.8 (c).

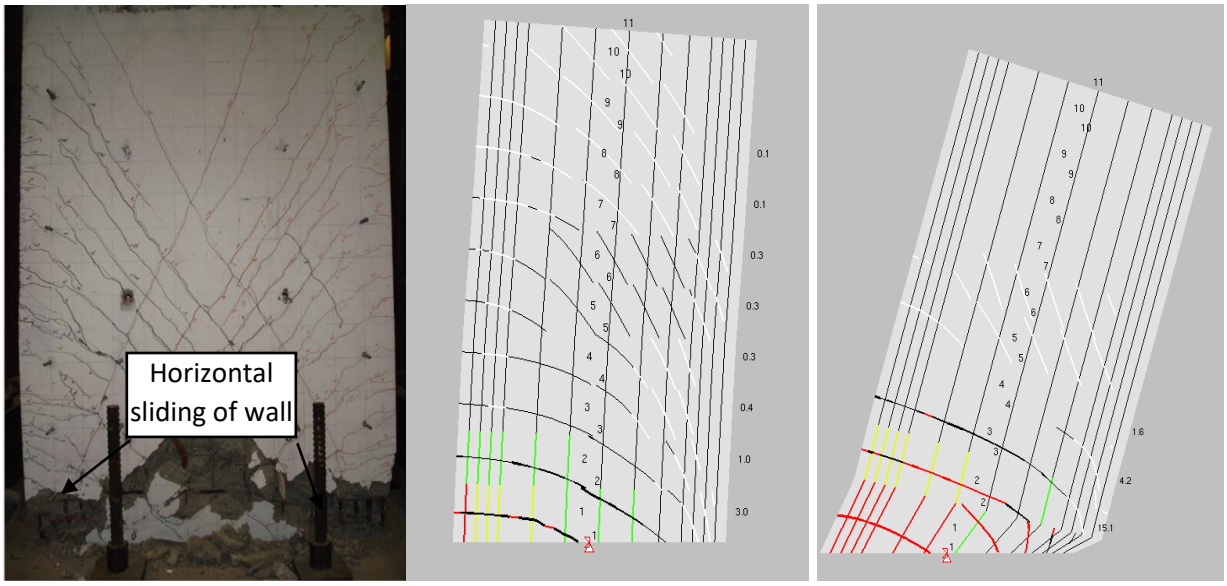

Fig 2.8 (a) Horizontal sliding failure; (b) Cracking pattern first yeilding; (c) Horizontal shear failure VecTor5.

2.2 Hube et al 2014

2.2.1 Experimental Program

Four half scale RC walls (W6–W9) were constructed and tested using a symmetric incrementally increasing cyclic lateral displacement test protocol with a constant axial load of 0.15 f'_c Ag. The test matrix is summarized in Table 2.3. The length (l_w) of the walls was 700 mm, and the thickness (t_w) was 100 mm. The thickness of the concrete cover was 10 mm and was the same for all specimens. The height of the walls (h_w) was 1600 mm. The walls were cast with a 425 x 400 x 1400 mm RC base to anchor them to the laboratory strong floor and with a 300 x 300 x 700 mm top RC beam to apply the vertical and lateral loads.

2.2.1.1 Material Properties

The dimensions and reinforcement detailing of RC walls are listed in Table2.3, taken from the experimental program done by Hube et al 2014.

Table 2.3 Wall specimen parameters (Hube et al 2014).

specimen	Author	h/lw	thickness	f'c		fy		ρflex %	ρh, %	ρv, %	P/Ag fc'
				Mpa	psi	Mpa	KSI				
W6	Hube et al 2014	2.5	100	27.4	3975	470	68.16	0	0.72	0.44	0.15
W7	Hube et al 2014	2.5	100	27.4	3975	470	68.16	0.45	0.72	0.44	0.15
W8	Hube et al 2014	2.5	100	27.4	3975	470	68.16	0.45	0.72	0.64	0.15
W9	Hube et al 2014	2.5	100	27.4	3975	470	68.16	0.45	0.72	0.56	0.15

The average concrete strength obtained from the standard cylindrical test was f'_c = 27.4 MPa. The samples were tested a day before the first wall test at an age of 160 days. The strength of concrete was assumed to have remained constant during the test campaign. The measured secant modulus of elasticity at 0.4 f'_c was E_c = 32,700 MPa. This modulus of elasticity is 33% larger than that proposed by ACI 318-08 ($Ec = 4700 (f'_c)^{1/2}$ = 24,600 MPa). The mean properties of the reinforcing steel are summarized in Table 2.4.

Table 2.4 Yield and ultimate strengths of reinforcement (Hube et al 2014).

Average properties of the reinforcing steel.

Parameter	∅4.2	∅5	∅8	∅10
Steel designation	AT560-500H	AT560-500H	A630-420H	A630-420H
Yield strength (MPa)	523.9	608.9	445.6	469.2
Ultimate strength (MPa)	575.7	667.7	598.9	675.7
Modulus of elasticity (GPa)	-	-	225.8	224.7
Yield strain	-	-	0.0020	0.0021
Hardening strain	-	-	0.0139	0.0138
Ultimate strain	0.0051	0.057	0.151	0.166
Strain Hardening modulus (MPa)	-	-	4130	5430

Note: The missing values were not measured during the tests of the reinforcing steel bars.

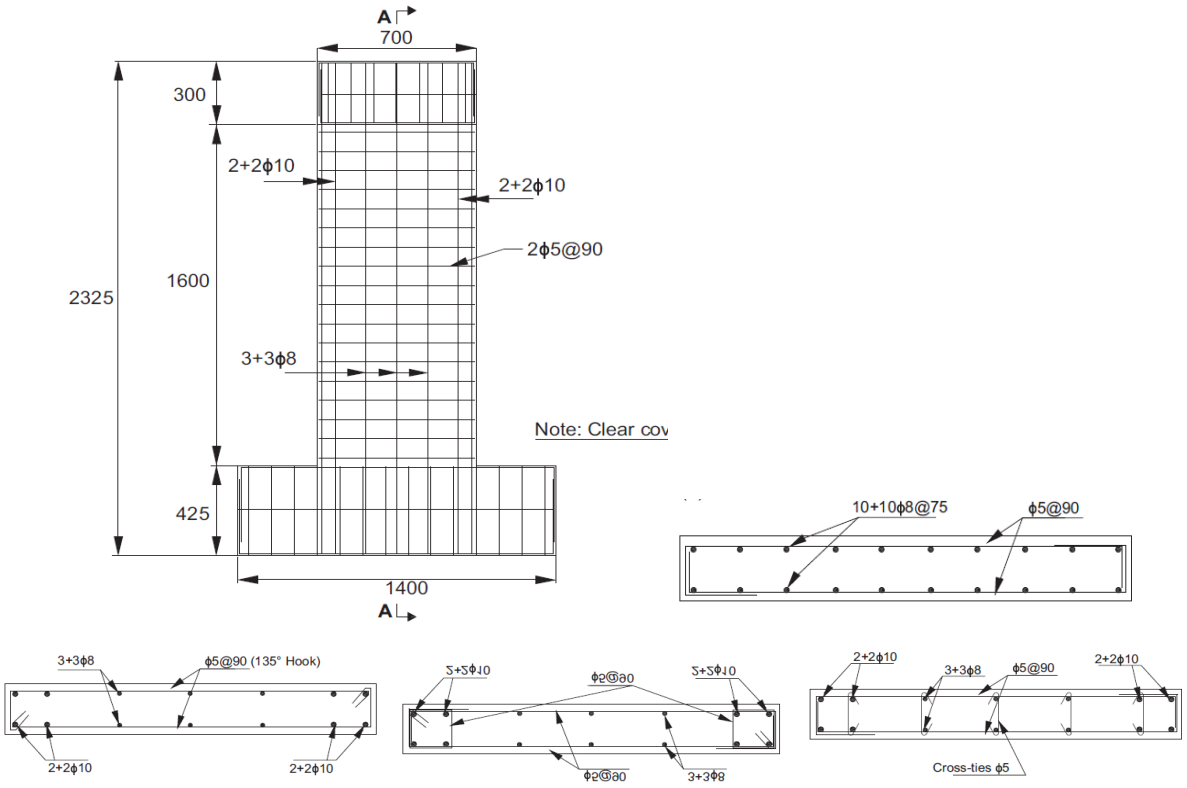

Figure 2.9 Dimensions and reinforcement details of wall specimens (Hube et al 2014).

2.2.1.2 Test Procedure

The test setup is shown in Figure 2.10 and the walls were pre-stressed to the laboratory floor at the base, and are considered as fixed at the interface to the specimen anchor block. 500 KN horizontal actuator was pinned at both ends and attached to the top RC beam with four steel bars that were bolted to 400 x 300 x 300 mm steel plates on each side of the specimen. The 700 KN vertical actuator was bolted to the steel frame and connected to the wall specimens using rollers to allow the horizontal displacement of the top RC beam. Therefore, the P-delta effect was not included in the test setup. The rotation of the top of the specimen was not restrained. A 5 KN concrete counter weight was connected to the clevis of the horizontal actuator using two pulleys. This counterweight was used to hang the actuator and eliminate the vertical reaction induced by its weight in the tested walls.

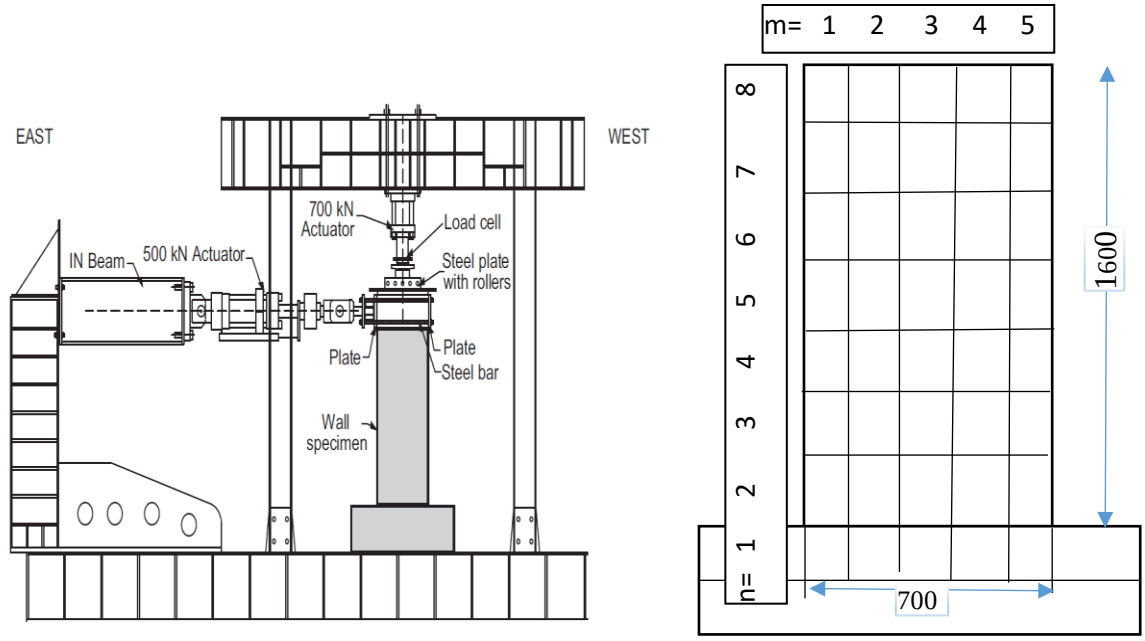

Figure 2.10 Experimental test set up (Hube et al 2014); (b) Model discretization in OpenSees.

2.2.2Numerical Modeling using OpenSees and VecTor5

Total horizontal top displacement (mm) vs horizontal load (KN) was obtained from the top-node of RC wall and the same procedure as (Tran and Wallace 2015), was done for three specimens for Hube 2014. A numerical modeling in OpenSees and VecTor5 with displacement control loading analysis was done and comparison of horizontal displacement (mm) vs horizontal load (KN) response is achieved as shown in Figure 2.11.

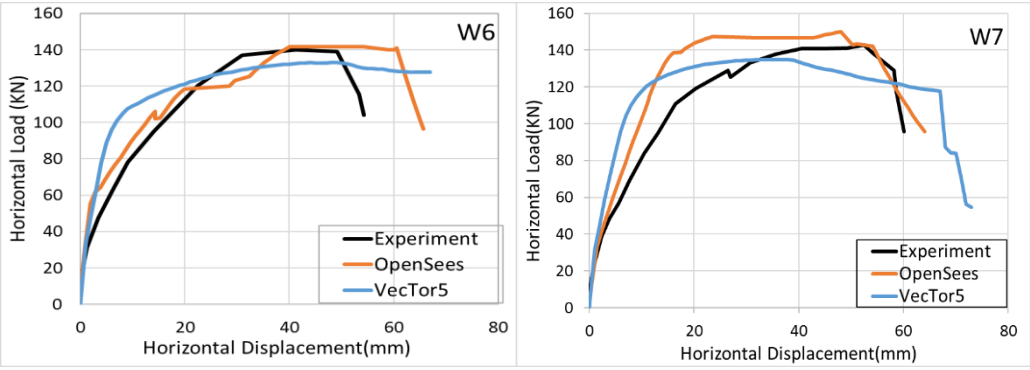

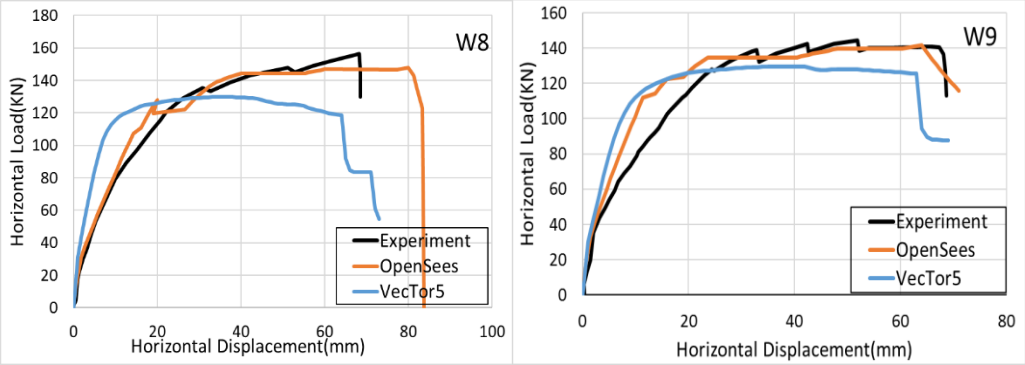

Figure 2.11 Comparison of horizontal displacement (mm) vs horizontal load (KN).

The behavior and failure of the walls were controlled by flexural-compressive interaction at the base of the wall due to the relatively high M/Vl_w ratio, like wise same flexural failure was observed from the VecTor5 analysis as shown in Figure 2.12.

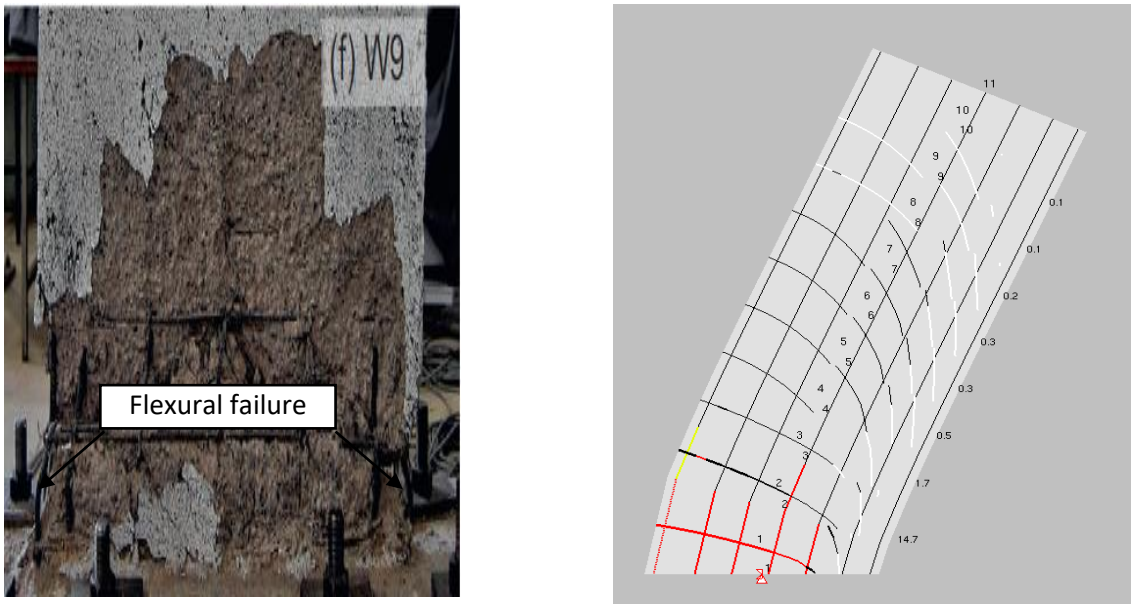

Figure2.12 (a) Flexural failure at the bottom of the wall; (b) Flexural failure observed inVecTor5.

2.3 Jang-Woon Baek et al 2017

2.3.1 Experimental Program

In this study, walls with h_w/l_w= 2.0 were experimentally tested to validate 550 MPa (80 ksi) reinforcing deformed bars for shear reinforcement. From the test, the essential structural capacities of walls with 550 MPa (80 ksi) reinforcing bars were measured. The experimental test results were directly compared with those of specimens with Grade 420 MPa (60 ksi) reinforcing bars, which

is currently specified as the maximum yield strength of shear reinforcement. These results can be used as evidence of the applicability of Grade 550 MPa (80 ksi) reinforcing bars to the shear design of slender walls.

Table 2.5 Wall specimen parameters (Jang-Woon Baek et al 2017).

specimen ID	Author	h/lw	thickness(mm)	f'c		fy		ρflex %	ρh, %	ρv, %
				Mpa	psi	Mpa	KSI			
HS2	Jang-Woon Baek et al 2017	2	200	36.5	5293	667	96.75	12.75	0.68	0.56
NS2L	Jang-Woon Baek et al 2017	2	200	36.5	5293	420	68.17	9.57	0.46	0.66
NF2	Jang-Woon Baek et al 2017	2	200	36.7	5322	420	68.17	10.56	0.93	1.08

Three wall specimens with the aspect-ratio of 2.0 were used for this project. The main test parameters are summarized in Table 2.5 including the grade of shear reinforcement (that is, horizontal and vertical web bars), reinforcement ratio to the gross concrete area, and failure mode. The names of the specimens indicate the primary test parameters. The first letters, N and H, refer to normal-strength bars (420 MPa [60 ksi]) and high-strength bars (550 MPa [80 ksi]) used for shear reinforcement, respectively. The second letters, S and F, refer to the failure mode of the specimens: shear failure mode and flexural yielding mode. The failure mode was controlled by the ratio of flexural reinforcing bars that were placed at the wall edges. The shear failure mode specimens were tested to investigate the magnitude of shear strength, and the flexural mode specimens were tested to investigate the effect of 550 MPa (80 ksi) shear bars on the shear strength degradation and wall ductility after flexural yielding. The third designation “2” indicates the aspect-ratio of the test specimens. In this test, all the specimens had an aspect-ratio of 2.0. The fourth letter, L, indicates a smaller shear bar ratio corresponding to around half of the maximum shear reinforcement ratio specified by ACI 349. For example, HS2L indicates a shear failure mode specimen with Grade 550 MPa (80 ksi) shear bars, an aspect-ratio of 2.0, and half of the maximum shear reinforcement ratio (Jang-Woon Baek et al 2017).

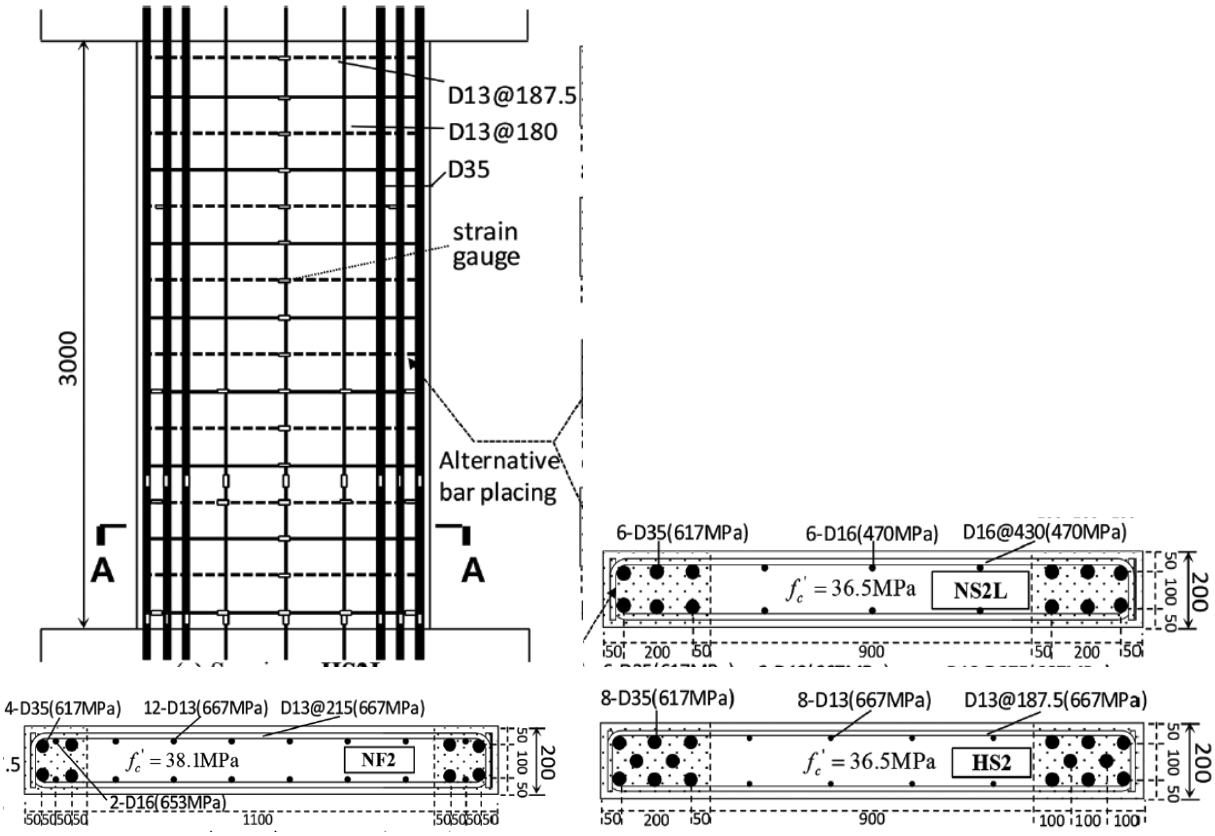

Figure 2.13 Dimensions and reinforcement details of specimens. (Note: 1 MPa = 0.145 ksi; 1 mm = 0.0394 in.).

2.3.1.1 Test Set Up

A cyclic lateral load and an axial compressive load and were applied using the test setup as shown in Figure 2.14 (a). Axial compressive load of approximately $0.07A_cf'_c$ (766 KN [172 kips] in the case of 36.5 MPa [5.29 ksi] concrete) was applied to the top of the wall by two displacement-controlled actuators. The level of the axial compressive force was maintained during cyclic lateral loading by manually controlling the vertical displacement. Generally, the actual level of axial load ratio for nuclear power plant walls ranges from 0.05 to 0.20 $A_cf'_c$.

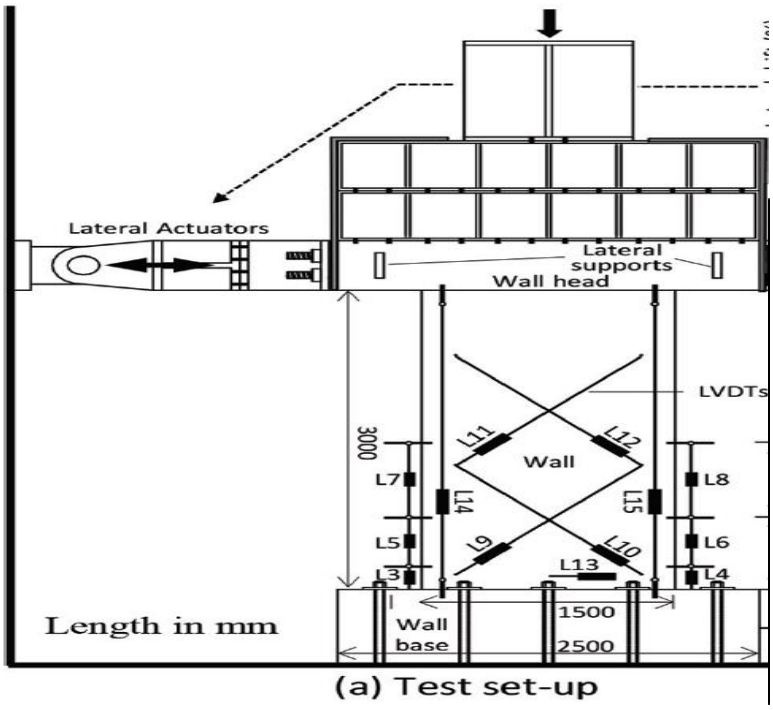

Figure 2.14 Experimental test set up

2.3.2 Numerical Modeling using OpenSees and VecTor5

Similar to the above experimental test (Tran and Wallace 2015), a numerical modeling in OpenSees and VecTor5 with displacement control loading analysis was done to capture maximum yielding capacity and failure mode of the RC walls and deflection response. A horizontal top displacement (mm) vs horizontal load (KN) was obtained from the top-node of RC wall and the same procedure as (Tran and Wallace 2015), was done for three specimens for Jang-Woon Baek et al 2017.

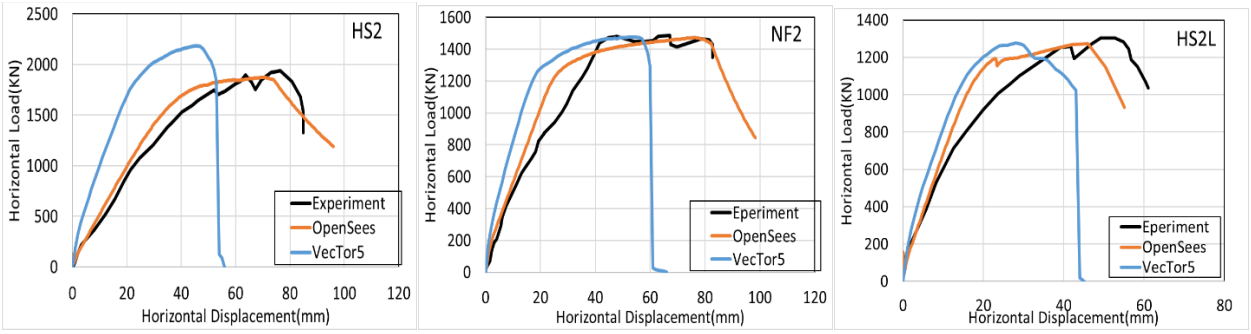

Figure 2.15 Comparison horizontal displacement (mm) vs Horizontal load (KN).

For comparison of failure modes for example HS2 RC wall of experimental test shows a first horizontal cracking which is flexural cracking along the boundary of the wall at 0.2 to 0.3 $h_{w,}$ then the horizontal crack propagates to a diagonal cracking along the web of wall at 0.3 to 0.5 h_w of the wall as shown in Figure 2.16(a) leads to shear failure of the RC wall, similarly the numerical modeling in VecTor5 shows the first yielding at the bottom of the wall as shown in Figure 2.16(b) with a shear failure mode at member 4 as shown in Figure 2.16(c).

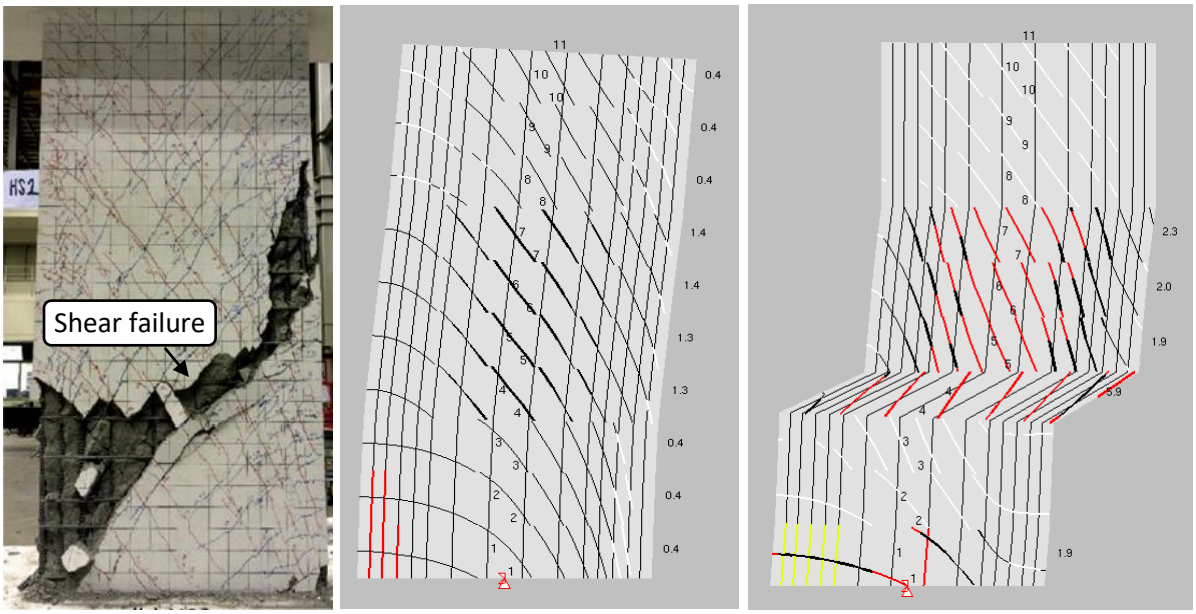

Figure 2.16 (a) HS2 Shear failure; (b) Cracking pattern at first yeilding; (c) Shear failure in VecTor5.

2.4 Discussion of Results PART I

A numerical modeling of ten moderate aspect RC walls was done in displacement control mode under monotonic loading condition in VecTor5 and OpenSees and comparison of peak load and horizontal displacement with the experimental test were done as shown in Table2.6. Comparing the ratio of VecTor5 and OpenSees to the experimental load, we got mean value 0.93 and 0.97 respectively, which is within the consistency range with the experiment though OpenSees give us the best load strength and in comparing the horizontal displacement both the numerical modeling software's give us less displacement comparing to the experiment with 1.03 of OpenSees to experiment ratio and 1.01 of VecTor5 to experiment ratio.

Table 2.6 Comparison of numerical modeling in OpenSees and VecTor5 with experimental results.

Monotonic Loading and Displacement Summary										
	Load (KN)					Displacement(mm)				
Name	Experimental	Opensees	VecTor5	POpen/Pexp	PVec/Pex	Experimental	Opensees	VecTor5	DOpen/Dexp	DVec/Dexp
HS2	1937.77	1875.93	2182.31	0.97	1.13	76.39	70.5	46	0.92	0.60
NS2L	1302.85	1274.25	1276.3	0.98	0.98	49.23	46.01	40	0.93	0.81
NF2	1485.4	1472.21	1477.25	0.99	0.99	67.04	76	60	1.13	0.89
R1.5_51	612.79	635.03	577.35	1.04	0.94	26.95	29.91	40	1.11	1.48
R1.5_64	671.87	702.43	703.73	1.05	1.05	36.02	37.8	47	1.05	1.30
R2.0_38	737.56	491.49	453.53	0.67	0.61	67.29	34.25	63	0.51	0.94
W6	140	141.55	132.86	1.01	0.95	41.25	54.29	46	1.32	1.12
W7	142.64	150.05	134.94	1.05	0.95	52.48	48	50	0.91	0.95
W8	156.59	147.64	130.03	0.94	0.83	68.29	80	64	1.17	0.94
W9	144.16	141.63	129.66	0.98	0.90	51.83	64.01	54	1.23	1.04
			mean	**0.97**	**0.93**			**mean**	**1.03**	**1.01**
			COV	**11.53**	**14.72**			**COV**	**22.12**	**24.66**

2.5 Summary and Conclusion

Numerical simulation of ten RC walls from three different experimental test programs under monotonic loading condition in OpenSees and VecTor5 was performed as Part I of this study. The main purpose of Part I was to deliver detailed information on the calibration of the multiple-vertical line element model (MVLEM) approaches in OpenSees and Modified Compression Field Theory (MCFT) and the Disturbed Stress Field Model (DSFM) formulation implemented on VecTor5 and present full correlation studies between the analytical expected and experimentally observed behavior of moderate aspect RC walls. Displacement-based formulation was used in both software's and the results of this studies conclude

- Overall Numerical modeling used in this study provides a good prediction of the experimentally observed responses (wall lateral load capacity, lateral stiffness, deflection response) in both OpenSees and VecTor5 programs. And also, failure modes obtained from VecTor5 are similar to the experimental test failure results

The authors recommend the modeling approach used in Part I of the study for comparison of lateral load capacity under monotonic loading for moderate aspect RC walls has the following limitation and that is the modeling method as shown in this paper for comparison studies of the experimentally observed response and predicted analytical values is proposed to stimulated only for load versus deflection curve response and effects of shear-flexural interaction are not considered.

PART II: Reverse Cyclic Loading

As Part II of this study, a reverse cyclic loading condition is applied to the above ten RC walls both in OpenSees and VecTor5. The effect of shear on moderate aspect-ratio RC walls and flexural capacity was achieved. In Part I given above, a two-dimensional Multiple-Vertical-Line-Element-Model (MVLEM) formulation implemented in OpenSees platform was used. And smeared, rotating crack approach based on the Modified Compression Field Theory (MCFT) and the Disturbed Stress Field Model (DSFM) formulation implemented on VecTor5 was used.

3.1 Experimental Program

Same geometry and material specification from the same three experimental test was done and used for monotonic loading as Part I are used for all the ten RC walls and the horizontal versus load curve is digitalized from their publications.

3.2 Modeling using OpenSees

To predict the maximum load capacity and effect of shear on the flexural capacity and failure modes of moderate aspect RC walls, all ten RC wall specimen from three experimental tests (Tran and Wallace 2015, Hube et al 2014, Jang-Woon Baek et al 2017), done before was selected and a nonlinear numerical modeling in OpenSees program under constant axial load and reverse cyclic loading was done. A displacement control pushover analysis is applied at the top of the wall and the lateral horizontal versus load response and failure models are achieved.

The same material specification as Part I of this study was used to model the RC walls and the nonlinear material response was defined using typical uniaxial concrete and steel response models as shown in Figure 1.3 (a) and (b) respectively. The Steel02 material model used to simulate the response of reinforcing uniaxial steel material. This model employs a bilinear envelope with unload-reload paths defined using Menegotto and Pinto (1973), the steel material object with isotropic strain hardening. And Concrete response was defined using uniaxial material ConcreteCM (Kolozvari et al., 2015), which is a uniaxial hysteretic constitutive model for concrete developed by (Chang and Mander 1994). The constitutive model for both steel and concrete materials used in this numerical modeling is shown in Figure 3.1.

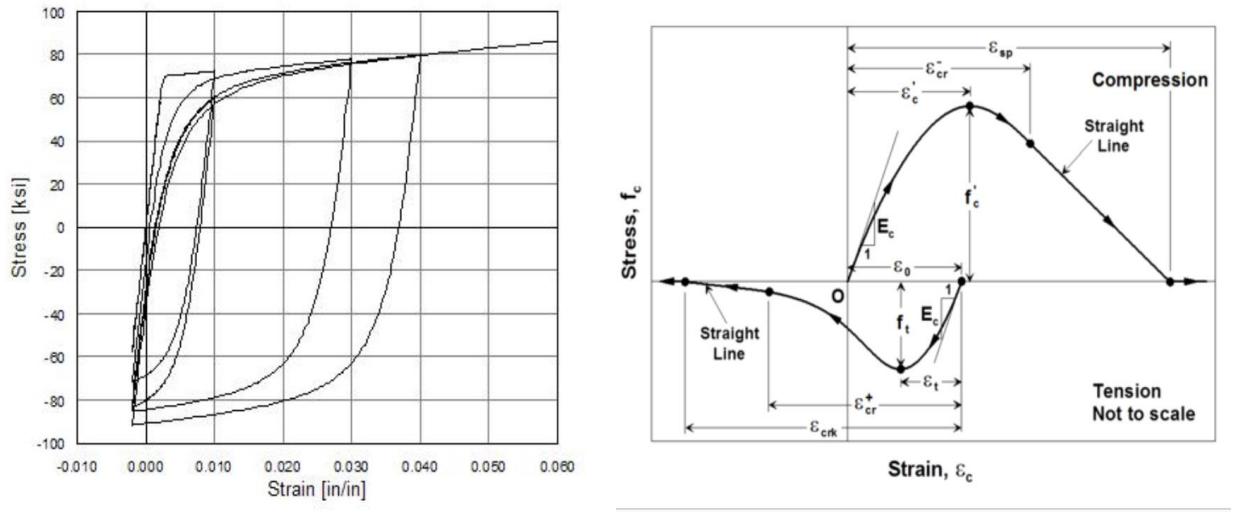

Figure 3.1 Uniaxial constitutive model for steel and concrete used in OpenSees.

3.3 **Modeling using VecTor5**

For experimental verification and comparing of the horizontal load versus displacement response, the RC walls also modeled in VecTor5. A Formworks Plus program, which is graphical interface that prepares the text files required for a VecTor5 program was used and the material properties and specifications are defined as experimental data used in Part I of this study. The concrete compressive strength, tensile strength, and other values of material behavior used are the same as Part I and can be defined in similar way as shown in Figure 2.5 and the transverse and longitudinal reinforcement can also be defined as shown in Figure 2.6 along with cross-sections for the members that will be meshed throughout the structure. The material behavior models used in VecTor5 to analysis under reverse cyclic loading conditions are defined in Table 3.1.

Table 3.1 Material behavior models used in VecTor5.

Concrete Behavior	Model	Rebar Behavior	Model
Compression Pre-Peak	Popovics (HSC)	Hysteresis	Seckin (w/ Bauschinger)
Compression Post-Peak	Popovics / Mander	Dowel Action	Tassios (Crack Slip)
Compression Softening	Vecchio 1992-A	Buckling	Modified Dhakal-Maekawa
Tension Stiffening	Modified Bentz 2003		
Tension Softening	Linear		
Confined Strength	Kupfer / Richard	**Analysis Options**	**Model**
Dilatation	Variable - Orthotropic	Geometric Nonlinearity	Considered
Cracking Criterion	Mohr-Coulomb	Shear Analysis Mode	Parabolic Shear Strain
Crack Width Check	Limit = Agg / 5	Shear Protection	On
Hysteresis	Nonlinear w/ Offsets	Convergence Limit	1.00001
Slip Distortion	Walraven	Maximum No of Iterations	100

In this Part, modeling of the RC walls in VecTor5, the VecTor.job file is the only one changed from monotonic to reverse cyclic loading shown in Figure 3.2.

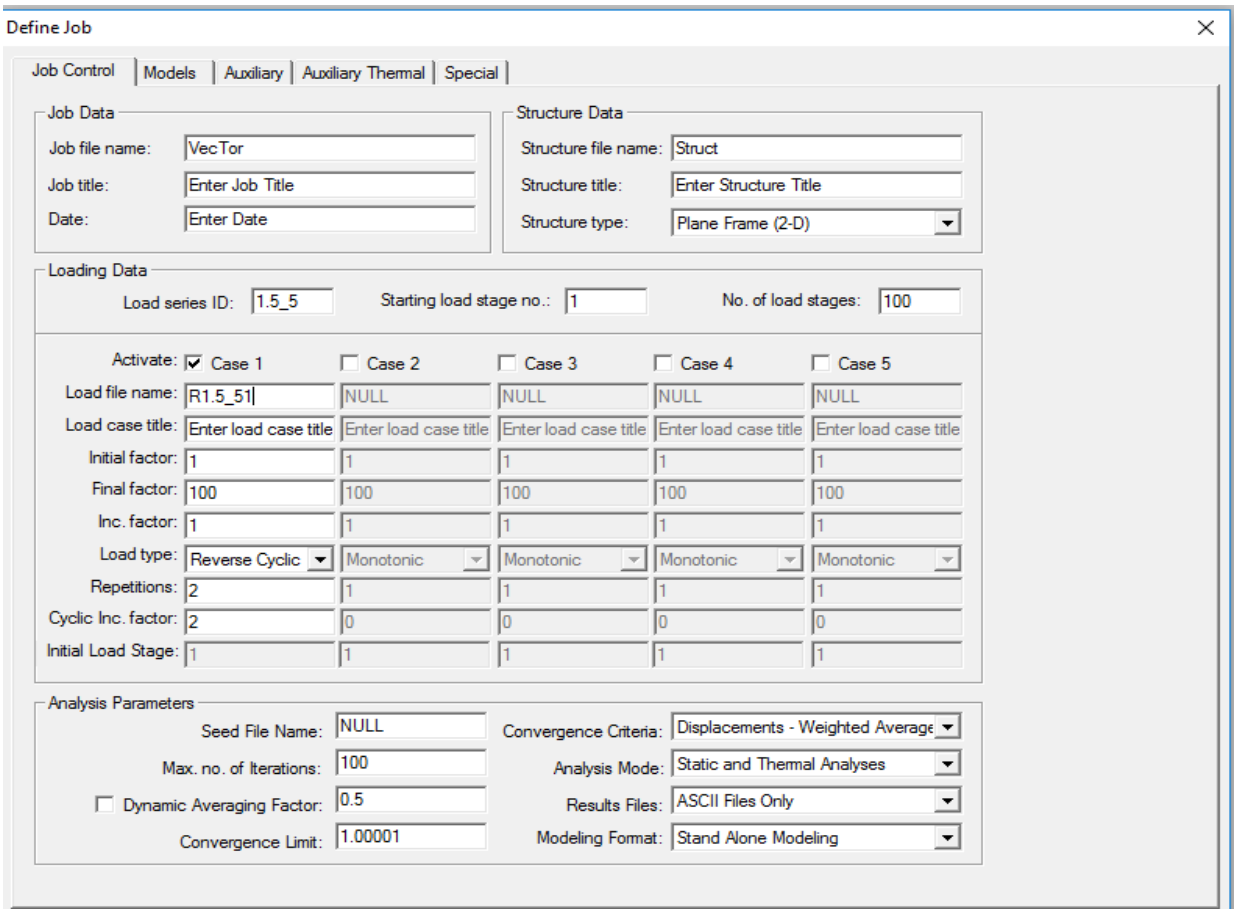

Figure 3.2 Vector Job file input parameter for cyclic loading.

Similar to Part I, the analytical modeling of the RC walls under cyclic loading in VecTor5 used a displacement control pushover analysis and a 3.0 mm horizontal displacement is applied at the top of the wall as a reversed cyclic load. For all the walls an increment of 1.0 and repeated for 2 cycle was applied before the load amplitude was increased by 6 mm as shown in Table 3.2.

Table 3.2 Reverse cyclic loading condition in VECTor5

No of Load Stage	200
Starting Load Stage no	1
Initial Factor	0.0
Final Factor	3.0
Ls-Increment	1.0
Types	3 (Reversed-cyclic
Reps	2
C-Inc	2

Similar to Part I of this study, in this Part, also the base blocks of the walls were not considered, rather they were modeled as a fixed supporter of the wall and no rigid zone used on all analysis using VecTor5 and (Seckin 1981), reinforcement materials model is used to stimulate the steel hysteresis. This model includes the Bauschinger effect, in which the reinforcement exhibits premature yielding upon load reversal after plastic pre-straining due to stress changes at the microscopic level as shown in Figure 3.3 (a). And for the concrete hysteresis, a nonlinear with offset is proposed by Vecchio that the unloading in the compression and tension domains follows nonlinear Ramsberg-Osgood formulations as shown in Figure 3.3.

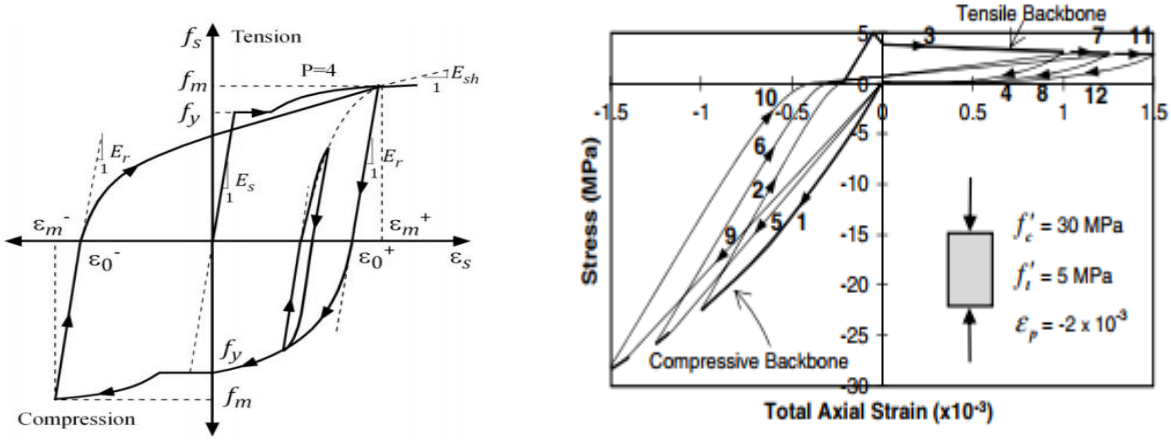

Figure 3.3 (a) Seckin w/ Bauschinger steel hysteresis; (b) Concrete hysteresis model

3.4 Comparison of Horizontal Load versus Displacement Curve

Total horizontal top displacement (mm) vs horizontal load (KN) was obtained from top-node of RC wall under reverse cyclic loading conditions from both OpenSees and VecTor5 simulations and comparison is done with the experimental response that is digitalized from the journal paper as shown in Figure 3.4.

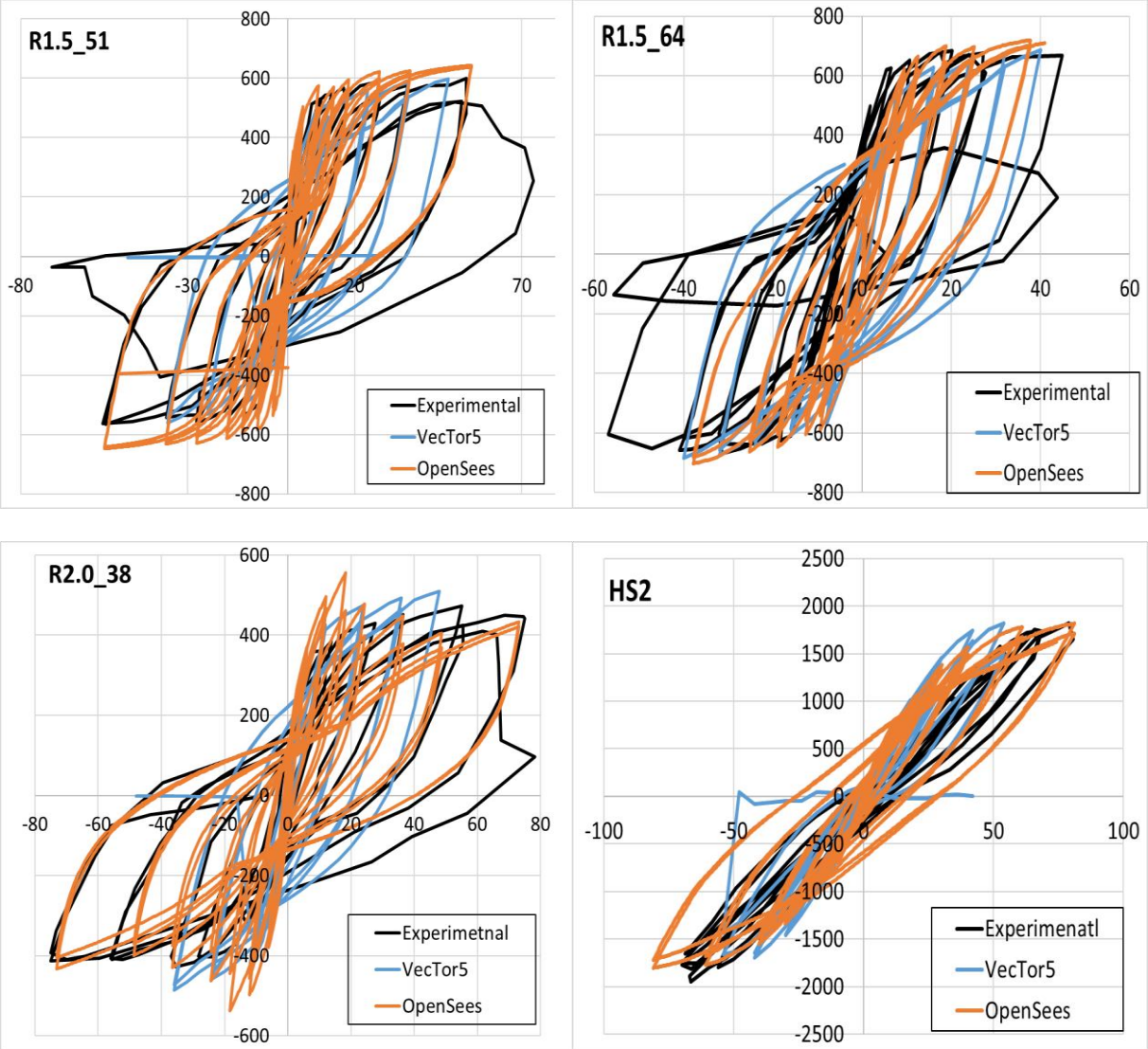

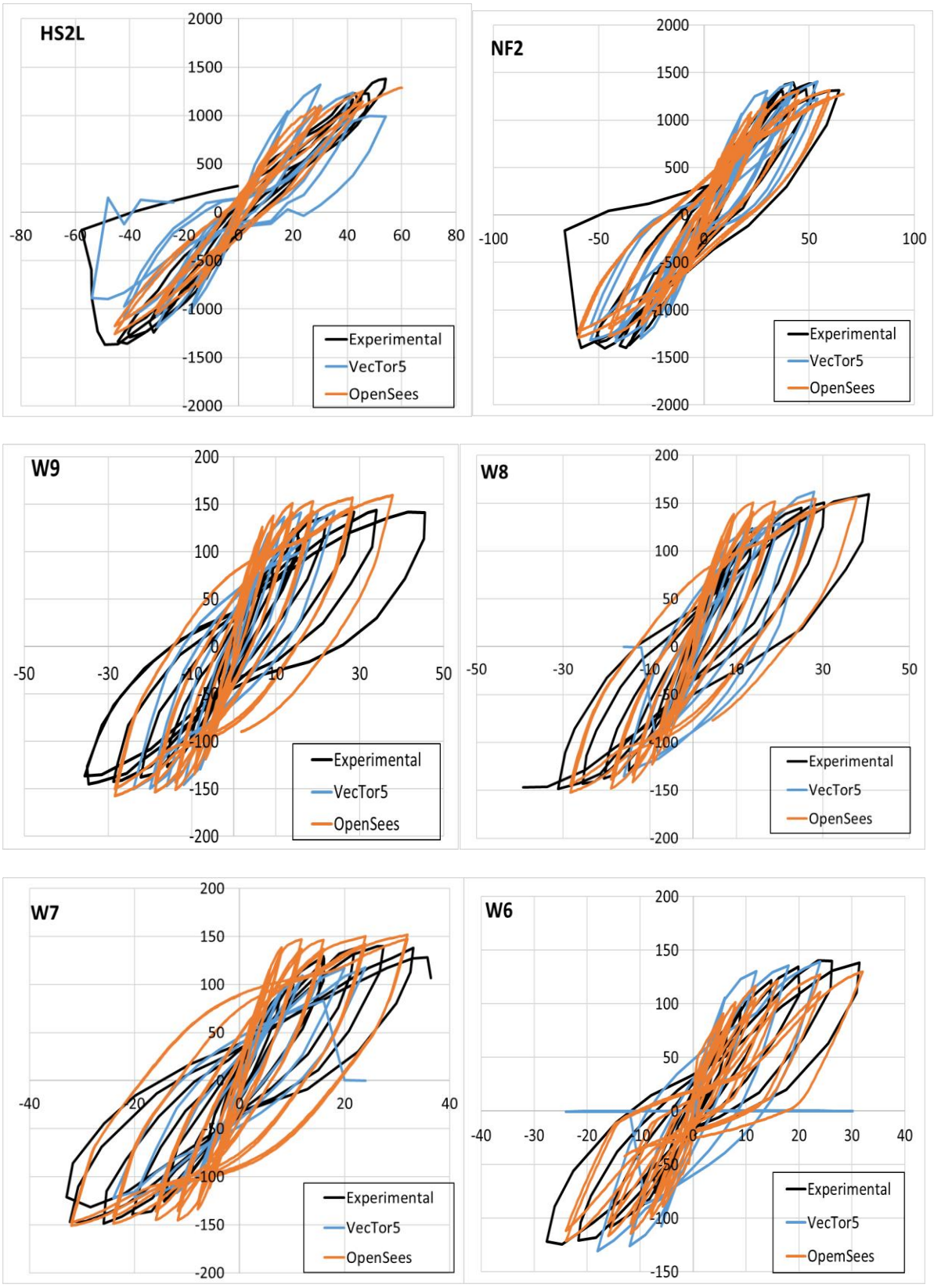

Figure 3.4 Comparison of horizontal displacement (mm) vs Horizontal load (KN).

As shown in Figure 3.4 the numerical modeling using OpenSees and VecTor5 captured reasonably well overall load-deformation response comparing to the experimental test done. And also as the purpose of this study is to predict failure modes of moderate aspect RC walls, a comparison of failure modes from Janus, post-processor of VecTor5, was done with the experimental failure modes as shown in Figure 3.5 below.

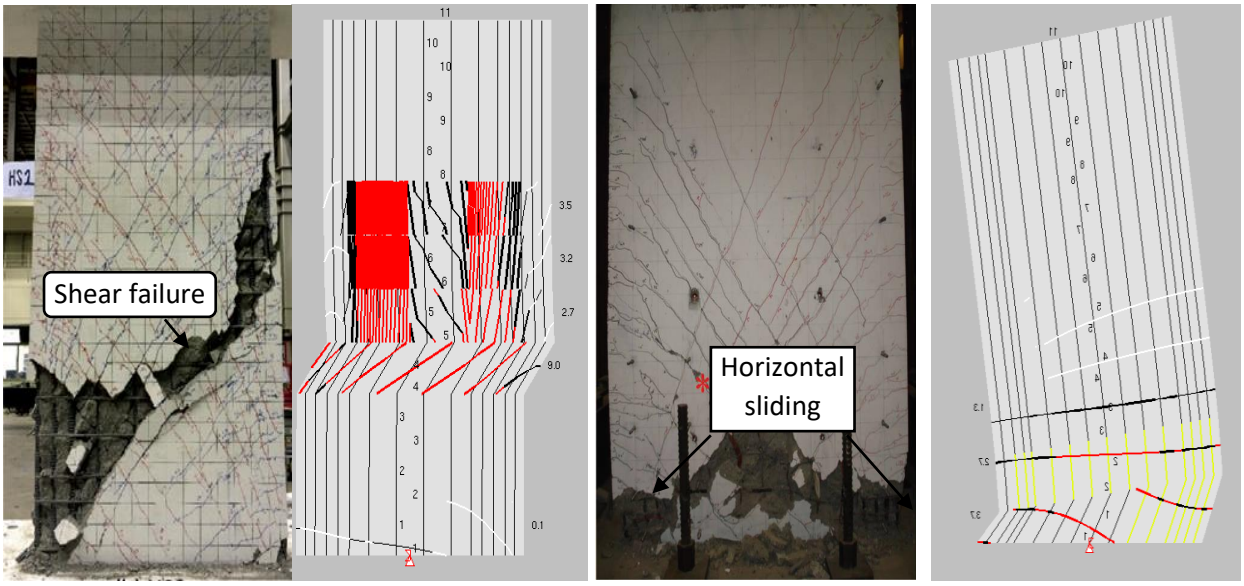

(a) HS2 Crack patterns and failure modes; (b) R1.5_51 Crack patterns and failure modes.

Figure 3.5 Comparison of failure modes experimental with the VecTor5 program.

3.5 Comparison of Experimental and Analytical Modeling Results

A numerical modeling of ten moderate aspect RC walls was done in displacement control mode under reverse cyclic loading condition in VecTor5 and OpenSees and comparison of positive and negative peak load and corresponding horizontal displacement with the experimental test were done as shown in Table3.3. Comparing the ratio of VecTor5 and OpenSees to the experimental load, we got mean value 0.99 and 1.03 respectively, with COV values of 7.35% and 8.88% which is within the consistency range. In this study, VecTor5 gave us the best load strength comparing to the experimental data and in comparing the horizontal displacement both the numerical modeling software's give us less displacement compared to the experiment with 0.93 of OpenSees to experiment ratio and 0.81 of VecTor5 to experiment ratio.

Table 3.3 Comparison of analytical and experimental results.

Reversed cyclic Loading and Displacement Summary											
		Peak load (kn)					Corresponding displacement(mm)				
Name		Experimental	Opensees	VecTor5	POpen/Pexp	PVec/Pexp	Experimental	Opensees	VecTor5	DOpen/Dexp	DVec/Dexp
HS2	positive	1822.16	1817.45	1823.3	1.00	1.00	76.39	81.12	54	1.06	0.71
	negative	-1946.92	-1803.46	-1797	0.93	0.92	-70.03	-81.02	-54	1.16	0.77
HS2L	positive	1302.85	1274.25	1317.5	0.98	1.01	49.23	56.08	54	1.14	1.10
	negative	-1370	-1288.82	-1184	0.94	0.86	-54.7	-45.61	-54	0.83	0.99
NF2	positive	1397	1314	1403.3	0.94	1.00	64	66.29	54	1.04	0.84
	negative	-1406	-1292	-1337	0.92	0.95	-64	-59.82	-54	0.93	0.84
R1.5_51	positive	599.05	643.85	598.57	1.07	1.00	63.43	54.86	44.8	0.86	0.71
	negative	-566.28	-648.13	-560	1.14	0.99	-60.62	-54.86	-48	0.90	0.79
R1.5_64	positive	684.15	718.47	684.9	1.05	1.00	44.85	40.95	40	0.91	0.89
	negative	-669.48	-703.22	-684.6	1.05	1.02	-56.94	-37.8	-40	0.66	0.70
R2.0_38	positive	473	555	509.57	1.17	1.08	67.29	73	56	1.08	0.83
	negative	-428	-538	-486.9	1.26	1.14	-75	-73	-56	0.97	0.75
W6	positive	140	130	139.21	0.93	0.99	31	32	30	1.03	0.97
	negative	-124	-121	-130.5	0.98	1.05	-28	-24	-24	0.86	0.86
W7	positive	139.69	152	127.75	1.09	0.91	36.43	32	28	0.88	0.77
	negative	-148.77	-151	-122.3	1.01	0.82	-32.94	-32	-28	0.97	0.85
W8	positive	159.04	155.42	161.97	0.98	1.02	40.6	37.8	28	0.93	0.69
	negative	-148.7	-152.32	-135.5	1.02	0.91	-39.22	-28.35	-28	0.72	0.71
W9	positive	143.62	159.33	143.03	1.11	1.00	45.47	37.8	28	0.83	0.62
	negative	-144.64	-157.09	-150.1	1.09	1.04	-35.66	-28.35	-28	0.80	0.79
				AVG	**1.03**	**0.99**			**AVG**	**0.93**	**0.81**
				COV	**8.88**	**7.35**			**COV**	**14.09**	**14.31**

3.6 Summary and Conclusion of Part II

Numerical simulation of ten RC walls from three different experimental test programs under reverse cyclic loading condition and constant axial load in OpenSees and VecTor5 was done as Part II of this study. The main purpose of Part II was to deliver detailed information on the calibration of the multiple-vertical line element model (MVLEM) approaches in OpenSees and Modified Compression Field Theory (MCFT) and the Disturbed Stress Field Model (DSFM) formulation implemented on VecTor5 present full correlation studies of shear effect on moderate aspect-ratio RC walls and flexural capacity between the analytical expected and experimentally observed behavior of moderate aspect RC walls and also to predict failure modes of moderate aspect-ratio RC walls. Displacement-based formulation was used in both software's and the results of this studies conclude,

- As shown in Figure 3.4, overall numerical modeling used in this study captured reasonably well where load-deformation behavior compared with the experimentally observed responses including wall lateral load capacity, lateral stiffness, and deflection response in both OpenSees and VecTor5 programs.

- Failure modes obtained from VecTor5 are similar to the experimental test failure results as shown in Figure 3.5 where numerical modeling predicted failure modes and orientation of cracks are in good agreement with the experimentally observed cracking pattern, indicating that the assumptions and modeling approached used are reasonable.
- The nonlinear analytical model successfully captured the shapes of the load versus flexural and shear deformation responses throughout the entire cyclic loading history and as demonstrated in the experimental conclusion, most of the RC walls from the analytical results also yielded around 70%-80% of the wall lateral capacity.

Summary and Conclusion

In this project, an analytical modeling of moderate aspect-ratio reinforced concrete walls that compare global nonlinear flexural, and horizontal displacement at the top of the wall was achieved both in OpenSees and VecTor5. A total of ten RC wall specimens, from experimental tests done in the past where from three different research programs are selected to model in this project which are divided into two parts. Part I of this project describes the analytical modeling of the RC walls under monotonic loading and Part II of this project describes the numerical modeling under reverse cyclic loading condition. In the nonlinear analysis of this project, a two-dimensional Multiple-Vertical-Line-Element-Model (MVLEM) formulation implemented in OpenSees platform was used. And also smeared, rotating crack approach based on the Modified Compression Field Theory (MCFT) and the Disturbed Stress Field Model (DSFM) formulation implemented on VecTor5 was used. A comparison of the simulated load capacities, horizontal displacement at the peak load, and the failure modes with the experimental results was done and the results of the studies conducted the following conclusions:

- The nonlinear numerical modeling analysis procedure predicted overall reasonably well load-deformation behavior response compared with the experimentally observed responses including wall lateral horizontal displacement at the top of the wall, stiffness, and shapes of the load versus displacement curve through bath monotonic and entire cyclic loading history in both OpenSees and VecTor5 programs.
- Failure modes obtained from VecTor5 captured similar to the experimental test failure modes and also orientation of cracks are in good agreement with the experimentally observed cracking pattern, indicating that the analytical modeling assumptions and modeling approached used are reasonable.
- Consideration of shear effects is important for moderate aspect-ratio RC walls as demonstrated in the experimental conclusion, most of the RC walls from the analytical results also yielded around 70%-80% of the wall lateral capacity and 90% of the analytical modeling shows a shear failure with diagonal cracking patterns similar to the experimental test.
- The author stated Pre- and post-processor software is essential in understanding the behavior and the failure mode of RC walls by showing the sequence of nonlinear events,

crack propagation, concrete and reinforcement stresses/strains, and the deflected shapes of the walls.

- The authors recommend the analytical modeling had a limitation of capturing failure modes form OpenSees as there was limitation in finding graphical interface that can show as failure modes obtained from OpenSees. So that failure modes obtained from numerical modeling are only captured from Janus post-processor of VecTor5 and compared with the experimental controlling failure modes.

REFERENCES

Birely AC. (2012). "Seismic performance of slender reinforced concrete structural walls," PhD dissertation. University of Washington; p. 983.

Pugh JS, Lowes LN, Lehman DE. (2015). "Nonlinear line-element modeling of flexural reinforced concrete walls," Engineering Structures. 104: 174-92.

Spacone E, Ciampi V, Filippou FC. (1996). "Mixed formulation of nonlinear beam-finite element," Comput Struct; 58(1):71–83.

Orakcal K, Wallace JW, Conte JP. (2004). "Flexural modeling of reinforced concrete walls – model attributes," ACI Struct J; 101(5): 688–98.

Orakcal K, Wallace J. Flexural (2006). "Modeling of reinforced concrete walls – experimental verification," ACI Struct J; 103(2): 196–206.

Leonardo M. Massone and John W. Wallace. (2004). "Load-deformation responses of slender reinforced concrete walls," ACI Struct J: 101-S12.

Ghobarah A, Galal G, Elgohary M. (2004). "Dynamic response of lightly reinforced concrete walls," Proceedings of the 13th world conference on earthquake engineering, Vancouver B.C., Canada. Paper No. 1090-2004.

Lai, S. S., Will, G. T. and Otani, S. (1984). "Model for inelastic biaxial bending of concrete member," Journal of Structural Engineering, ASCE, 110:11, 2563-2584.

Galal K. (2008). "Modeling of lightly reinforced concrete walls subjected to near-fault and far-field earthquake ground motions," Struct Des Tall Special Buildings; 17: 295–312.

Vulcano A, Bertero VV, Colotti V. (1988). "Analytical modeling of RC structural walls," Proceeding 9th world conference on earthquake engineering, V. 6, Tokyo, Kyoto, Japan. p. 41–60.

Guner, S., 2008, "Performance assessment of shear-critical reinforced concrete plane frames," PhD thesis, Department of Civil Engineering, University of Toronto, Toronto, ON, Canada, 429 pp.

Guner, S., and Vecchio, F. J., 2008, "User's manual of VecTor5," Online Publication, 88 pp.

Guner, S., and Vecchio, F. J., 2011, "Analysis of shear-critical reinforced concrete plane frame elements under cyclic loading," Journal of Structural Engineering, ASCE, V. 137, No. 8, pp. 834-843.

Vecchio, F., J. (1989). “Nonlinear finite element analysis of reinforced concrete membranes,” ACI Structural Journal, 86:1, 26-35.

Jiang H, Kurama Y. (2010). “Analytical modeling of medium-rise reinforced concrete shear walls,” ACI Struct J 107 (4):400–10.

Calugaru V, Panagiotou M. (2012). “Response of tall cantilever wall buildings to strong pulse type seismic excitation,” Earthquake Eng Struct Dynam; 41:1301–18.

Li, K. N. (2006). “Three dimensional nonlinear static and dynamic structural analysis computer programs,” User’s Manual, CANNY Structural Analysis, Vancouver, BC, Canada.

Panneton M, Leger P, Trembley R. (2006). “Inelastic analysis of a reinforced concrete shear wall building according to the National Building Code of Canada 2005,” Can J Civ Eng; 33(7):854–71.

Petrangeli M. (1999). “Fiber element for cyclic bending and shear of RC structures II: verification,” J Eng Mech; 125(9):1002–9.

Bazant Z, Oh B. (1985). “Microplane model for progressive fracture of concrete and rock,” ASCE J Eng Mech; 111:559–82.

Bazant Z, Ozbolt J. (1990). “Nonlocal microplane model for fracture, damage and size effect in structures,” ASCE J Eng Mech; 116(11):2484–504.

Bazant Z, Prat P. (1988). “Measurement of mode III fracture energy of concrete,” Nucl. Energy Des; 106:1–8.

Ozbolt J, Bazant Z. (1992). “Microplane model for cyclic triaxial behavior of concrete,” ASCE J Eng Mech; 118(7):1365–86.

Bentz EC. (2000). “Sectional analysis of reinforced concrete members,” PhD thesis. Department of Civil Engineering, University of Toronto; p. 310.

Vecchio F, Collins M. (1986). “The modified compression-field theory for reinforced concrete elements subjected to shear,” ACI Struct J; 83(2):219–3.

Palermo D, Vecchio F. (2007). “Simulation of cyclically loaded concrete structures based on the finite-element method,” ASCE J Struct Eng; 133(5):728–38.

Palermo D, Vecchio FJ. (2002). “Behavior of three-dimensional reinforced concrete shear walls,” ACI Struct J; 99(1):81–90.

Oesterle, R. G., Aristizabal-Ochoa, J. D., Shiu, K. N. and Corely, W. G. (1984). “Web crushing of reinforced concrete structural walls,” ACI journal Proceedings, 81:3, 231-241.

Kolozvari K, Orakcal K and Wallace J (2015). “Shear-flexure interaction modeling for reinforce concrete structural walls and columns under reversed cyclic loading,” PEER report No.2015/12.

M. Panagiotou, J. I. Restrepo, M. Schoettler, and G. Kim (2012). “Nonlinear cyclic truss model for reinforced concrete walls,” ACI Strut J. 109(2): 205-214

Tasnimi A. A (2000). “Strength and deformation of mid-rise shear walls under load reversal,’’ Engineering Structures 22 311–322.